THESIS FOR THE DEGREE OF DOCTOR OF PHILOSOPHY

Mooring Dynamics for Wave Energy Applications

A high-order discontinuous Galerkin method for cables, coupled to Reynolds averaged Navier-Stokes simulations.

JOHANNES PALM

Department of Shipping and Marine Technology
CHALMERS UNIVERSITY OF TECHNOLOGY
Gothenburg, Sweden
2017

Mooring Dynamics for Wave Energy Applications

A high-order discontinuous Galerkin method for cables,
coupled to Reynolds averaged Navier-Stokes simulations.

JOHANNES PALM
ISBN: 978-91-7597-562-7

Doktorsavhandlingar vid Chalmers tekniska högskola
Ny serie nr. 4243
ISSN 0346-718X

Department of Shipping and Marine Technology
Chalmers University of Technology
SE-412 96 Göteborg
Sweden
Telephone + 46 (0)31-772 1000

Printed by Chalmers Reproservice
Göteborg, Sweden 2017

Mooring Dynamics for Wave Energy Applications
A high-order discontinuous Galerkin method for cables, coupled to Reynolds averaged Navier-Stokes simulations.
JOHANNES PALM, 2017
Department of Shipping and Marine Technology, Chalmers University of Technology

ABSTRACT

This work aims to increase the modelling accuracy of two important problems for the wave energy industry. One concerns the mooring dynamics in the presence of snap loads (shock waves in cable tension). The other is related to nonlinear effects in the resonance region of moored wave energy converters (WECs).

The thesis describes the development of Moody, a high-order discontinuous Galerkin (DG) model for mooring dynamics aimed at capturing snap loads. Two different DG formulations are presented. The first version uses the local DG method, while the second is based on the Lax-Friedrich (LF) approximative Riemann solver. Exponential convergence for smooth cases and excellent agreement with experimental data are shown for both versions. The LF-based solver is extended to include shock-identifiers, slope limiters and $hp-$adaptive mesh refinement. Computational results show good shock resolution in both linear and nonlinear cable materials. We further develop an automated program interface to provide dynamic mooring response to volume of fluid Reynolds averaged Navier-Stokes (VOF-RANS) simulations of WECs in OpenFOAM®.

Model scale experiments of a moored vertical cylinder are carried out with the partial aim to provide validation data for the coupled VOF-RANS-Moody model. The validation shows very good agreement between experimental and numerical results of surge and heave motion, from which we conclude that the coupling is working as expected. We get a good match in mooring force response, but the pitch response is shown to be more sensitive to model input parameters. Validation of high-fidelity models puts tough requirements on experimental data quality, which are difficult to meet in small scales.

The experiments also assess the performance of three types of mooring configurations for WECs. Results show how cable slack-snap events are important for the dynamic range of mooring force response in survival conditions. As the steepness of the waves increase, the response amplitude per wave height decreases in the resonance region for all three configurations. This nonlinear effect is consistently seen throughout the results from experiments and coupled simulations of both model scale and full-scale geometries. Although paid for with a substantial computational effort, we conclude that the high-fidelity VOF-RANS-Moody model is able to predict the fully nonlinear response of WECs with good accuracy.

Keywords: Mooring dynamics, Wave energy, Snap loads, Discontinuous Galerkin methods, $hp-$adaptivity, CFD, OpenFOAM, RANS, Coupled simulations

Till mamma och pappa

PREFACE

I was first introduced to wave energy utilization in 2010 when I, in search of a Master thesis project on renewable energy, had a tip on a mooring project with WEC developer Waves4Power and Reinertsen technical consultants. I went to see the supervisor, Prof. Lars Bergdahl. Two minutes later I had been given John Fitzgerald's freshly printed thesis on position mooring of wave energy converters, to read over night as *Lasse* expected to know if I was interested already the next day. None the wiser I went home, started reading the thesis, realised that I did not understand it, and went back to Lasse's office the next day and said that I would gladly do the project.

I began my PhD studies at the department of Shipping and Marine Technology in 2012. During this time I have been embarrassingly secluded in my office trying to get computer code to run as I expected it to, and I apologize to all my colleagues at the department for not taking the time to get to know you better than I have. I have struggled quite hard with my own expectations on what it means to *be a Doctor*, and I have many times sadly reflected on the futility of my efforts in comparison with the vast amount of high-quality research being produced in the world. However, I have found comfort in the occasional updates from Research Gate appearing in my e-mail inbox:

A researcher from Portugal read your work last week.

Often it has in fact been a co-author who found it quicker to look up our joint paper online than to use a local copy, but the confidence boosts have been mine to keep in blissful ignorance of the fact.

A special acknowledgement must be given to Guilherme Moura Paredes. We have worked closely, particularly during 2012-2013 when we shared office both here at Chalmers and at the university of Porto. The little knowledge I have gained in experimental work is much due to you and our joint efforts in the hydraulics lab in Porto, on those occasional days when the equipment worked as expected. This thesis would not have been the same without you.

I have had great support in this thesis work. Not only have my main supervisor Doctor Claes Eskilsson, the co-supervision of Prof. Lars Bergdahl and the support from Prof. Rickard Bensow given me excellent guiding in the craftsmanship of research, they have also provided a creative and collegial atmosphere to work in. For this, and for many fine memories over the years, I am deeply thankful. I have had the privilege of working very closely with Claes throughout this whole process. Your contributions to the work presented herein and your part in the knowledge I have gained have been absolutely essential. Thank you.

Till sist, all min kärlek till Frida och Ottilia. Ni är och förblir viktigast.

Johannes Palm
Göteborg, 2017-04-10

ACKNOWLEDGEMENTS

Funding for this work is gratefully acknowledged to the following agencies and institutions.

- Västra Götalandsregionen (VGR) for support through the Ocean Energy Centre.
- The Swedish Energy Agency (SEA) for support of two projects on wave energy conversion: (i) quantification of nonlinear and viscous loads on wave energy converters, project number P40428-1; and (ii) the newly started work on prediction and mitigation of snap loads in mooring cables, project number P42246-1.
- Adlerbertska forskningsstiftelsen for supporting my three month stay in Porto and the experimental work of this thesis.
- The EUDP funding program that enabled my participation in the SDWED project, lead by Aalborg University.
- The department of Shipping and Marine Technology at Chalmers, whose internal funds I slowly depleted for a period of time.

The computational fluid dynamics (CFD) simulations of moored wave energy converters presented in this work would not have been possible without the computational resources provided by the Swedish National Infrastructure for Computing (SNIC) at the Chalmers Centre for Computational Science and Engineering (C3SE), and at the National Supercomputer Centre (NSC).

List of papers

This thesis is compiled from the work presented in the following five papers, referred to with roman numerals in the text:

I J. Palm, G. Paredes, C. Eskilsson, F. Taveira-Pinto, and L. Bergdahl. Simulation of mooring cable dynamics using a discontinuous Galerkin method. In *Proc. 5th International Conference on Computational Methods in Marine Engineering*, Hamburg, Germany, 2013

II J. Palm, C. Eskilsson, G. Paredes, and L. Bergdahl. CFD simulations of a moored floating wave energy converter. In *Proc. 10th European Wave and Tidal Energy Conference*, Aalborg, Denmark, 2013

III G. Paredes, J. Palm, C. Eskilsson, L. Bergdahl, and F. Taveira-Pinto. Experimental investigation of mooring configurations for wave energy converters. *Int. J. of Marine Energy*, 15:56–67, 2016

IV J. Palm, C. Eskilsson, G. Paredes, and L. Bergdahl. Coupled mooring analysis for floating wave energy converters using CFD: Formulation and validation. *Int. J. of Marine Energy*, 16:83–99, 2016

V J. Palm, C. Eskilsson, and L. Bergdahl. An hp-adaptive discontinuous Galerkin method for modelling snap loads in mooring cables. *Submitted*, pages 1–32, 2017

Contribution to papers

I have been the main author of papers I, II, IV and V. I have also been the main developer of the computer code for mooring dynamics used in the simulations. Paper I and Paper III were written in close collaboration with Guilherme Moura Paredes. I took active part in planning and designing the experiments presented in Paper III, and I participated in three months of laboratory testing at the department of Civil Engineering, University of Porto. Both the analysis of the results and the writing of the paper were joint efforts.

OTHER PUBLISHED WORK

In addition to the appended papers, I have authored or co-authored the following publications/reports during my PhD studies:

- J. Palm. *Connecting OpenFOAM with MATLAB*, 2012. Available http://www.tfd.chalmers.se/~hani/kurser/OS_CFD_2012/
- G. Paredes, C. Eskilsson, J. Palm, L. Bergdahl, L. Leite, and F. Pinto. Experimental and numerical modeling of a moored, generic wave energy converter. In *Proc. 10th European Wave and Tidal Energy Conference*, Aalborg, Denmark, 2013
- G. Paredes, L. Bergdahl, J. Palm, C. Eskilsson, and F. Pinto. Station keeping design for floating wave energy devices compared to floating offshore oil and gas platforms. In *Proc. 10th European Wave and Tidal Energy Conference*, Aalborg, Denmark, 2013
- G. Paredes, J. Palm, C. Eskilsson, L. Bergdahl, and F. Taveira-Pinto. Numerical modelling of mooring systems for floating wave energy converters. In *8as Jornadas de Hidráulica, Recursos Hídricos e Ambiente*, Porto, 2014. Faculdade de Engenharia da Universidade do Porto
- J. Palm and C. Eskilsson. *MOODY, User's manual version m-1.0*, 2014. Avaliable www.sdwed.civil.aau.dk
- J. Palm. Developing Computational Methods for Moored Floating Wave Energy Devices. Technical report, Department of Shipping and Marine Technology, Chalmers University of Technology, 2014. Lic.Eng. Thesis. Report No. 14:151
- J. Palm, C. Eskilsson, G. Paredes, and L. Bergdahl. CFD study of a moored floating cylinder: Comparison with experimental data. In C. Guedes Soares, editor, *Renewable Energies Offshore*, pages 913–920. Taylor & Francis Group, November 2014
- C. Eskilsson, J. Palm, J.P Kofoed, and E. Friis-Madsen. CFD study of the overtopping discharge rate of the Wave Dragon wave energy converter. In C. Guedes Soares, editor, *Renewable Energies Offshore*, pages 287–294. Taylor & Francis Group, November 2014
- F. Ferri and J. Palm. Implementation of a dynamic mooring solver (MOODY) into a wave to wire model of a simple WEC. Technical report, Department of Civil Engineering, Aalborg University, 2015

- C. Eskilsson, J. Palm, A.P. Ensig-Karup, U. Bosi, and M. Ricchiuto. Wave induced motions of point-absorbers: an hierarchical investigation of hydrodynamic models. In *Proc. 11th European Wave and Tidal Energy Conference*, Nantes, France, 2015
- G. Paredes, J. Palm, C. Eskilsson, L. Bergdahl, and F. Taveira-Pinto. Experimental investigation of mooring configurations for wave energy converters. In *Proc. 11th European Wave and Tidal Energy Conference*, Nantes, France, 2015
- S. Yang, J. Ringsberg, E. Johnson, Z. Hu, and J. Palm. A comparison of coupled and de-coupled simulation procedures for the fatigue analysis of wave energy converter mooring lines. *Ocean Engineering*, 117:332–345, 2016
- L. Bergdahl, J. Palm, C. Eskilsson, and J. Lindahl. Dynamically scaled model experiment of a mooring cable. *J. Marine Science and Technology*, 4(5), 2016
- J. Palm, C. Eskilsson, and L. Bergdahl. Mooring cable simulations with snap load capturing for wave energy applications. In C. Guedes Soares, editor, *Progress in Renewable Energies Offshore*, pages 695–701. Taylor & Francis Group, October 2016

COLLABORATION

The project has included collaboration with three foreign universities: Aalborg University (AAU), the engineering faculty at the University of Porto (FEUP), and Instituto Superior Téchnico (IST), Lisbon. The finite element model for moorings developed in this thesis has been used in two dissertations. See the work of Guilherme Moura Paredes [122] at (FEUP) and the work of Pedro Vicente [161] at IST.

CONTENTS

1 Introduction 1
1.1 The wave energy industry 2
1.1.1 Historical development 2
1.1.2 A new generation 4
1.2 Motivation 5
1.2.1 Design considerations 5
1.2.2 Mooring challenges 7
1.3 Aim 8
1.4 Scope 9
1.5 Structure of the thesis 10

2 Hydrodynamic modelling of WECs 11
2.1 Water waves 11
2.2 Method of choice 13
2.2.1 VOF-RANS 13
2.2.2 Floating bodies 14
2.3 VOF-RANS versus wave-to-wire models 15
2.4 Review of high-fidelity WEC models 16

3 Mooring dynamics 21
3.1 Mooring overview 21
3.1.1 List of demands 21
3.1.2 Mooring materials 23
3.1.3 Previous studies 23
3.1.4 Configurations 24
3.2 Cable dynamics 26
3.2.1 Coordinate systems 26
3.2.2 Equation of motion 27

3.2.3 External forces 28
3.2.4 Strain measures 30
3.3 Snap loads 30
3.4 Numerical models of cables 31

4 The discontinuous Galerkin method 33
4.1 Background 33
4.2 DG for a model problem 34
4.2.1 Nodal or modal basis 35
4.2.2 The numerical flux 36
4.3 The local discontinuous Galerkin Method 37
4.4 Shock capturing techniques 38
4.5 Adaptivity 39

5 Summary of work 41
5.1 Software development 41
5.2 A local discontinuous Galerkin formulation - Paper I 44
5.3 Coupled CFD-mooring analysis - Paper II 45
5.4 Experimental work - Paper III 46
5.5 Validation of the coupled model - Paper IV 49
5.6 Capturing snap loads - Paper V 51
5.7 Further mooring studies 52

6 Discussion 55
6.1 Modelling mooring dynamics 55
6.2 Experimental data for validation 58
6.3 VOF-RANS simulations 59
6.4 Coupled CFD-mooring analysis 61
6.5 The role of VOF-RANS in WEC design 61

7 Concluding remarks 63

References 65

1

Introduction

It is easy to make a device that will respond
vigorously to the action of sea waves.
Indeed, it is quite hard to make one that will not.
Salter, Taylor and Caldwell [142].

Wave power as a source of clean and reliable energy is today an actively studied topic in the quest for an ecologically sustainable society. In 2014, the total world consumption of electric energy was 19800 TWh/year [2], with a global wave energy resource of the same magnitude [40]. Estimations of techically available wave energy potential on a global scale are however commonly placed between 2000 to 4000 TWh/year [3]. The key phrase here is of course *technically available* and how it is defined. The wave power industry is still evolving, and estimations of cost of energy over long periods of time are therefore volatile. This makes it difficult to pinpoint which areas that can sustain commercial wave power installations. Future technological developments and/or socio-economic changes might enable usage of a larger (or smaller) portion of the total wave energy resource.

The Ocean Energy Systems annual report of 2015 [149] envisions 337 GW of installed power from ocean energy (including waves, tidal currents, tidal ranges, salinity gradients and ocean thermal energy) by 2050. The contribution from wave and tidal current energy in Europe alone should by then be 100GW [150]. In June 2016, the installed wave power capacity in Europe was 5MW, with another 7MW from tidal currents [66]. Clearly there is a long way to go. However, the current roadmap of the Ocean Energy Forum [66] suggests industrial roll-out of wave energy devices to ramp up from year 2030. Wave power can have a substantial impact on the energy system and aid in the societal transformation away from fossil fuel dependency. But, it is not the holy grail of energy and we should pursue it with the understanding that wave energy is a complementary source of energy, to be combined with others in the family of renewable energy: solar, wind, and tidal energy, not forgetting the well-established hydro-power industry.

This thesis aims to increase the accuracy of numerical models used to design moored wave energy converters (WECs). The motivation for the research is nested in the wave energy industry, its engineering challenges and its technological development path.

1.1 The wave energy industry

As the quote at the start of the chapter suggests, it is intuitive to think of a device that will absorb power from the waves. But that does not make it simple to build a good one. The demands and design constraints on wave energy installations are many and require multi-disciplinary competences. Apart from the detailed engineering of the device itself, its internal mechanisms and functionality, one must also consider e.g. the effect on marine life [39], grid connection rules on power quality [159], proximity to shore and weather windows for operation and maintenance (O&M), foundations and sea-bed conditions [170], and issues of legislation [109]. To maximise power output, WECs are designed to absorb the maximum amount of energy from the waves, and they are ideally placed in areas of high incoming wave energy density. The WEC structure is therefore exposed to large wave loads, which increases the material costs needed to ensure survival of the device. At the same time, financial considerations are strained by costly offshore operations and by the low price on the electricity produced. Therefore, a WEC that works is simply not enough. It needs to work with a near-optimum efficiency and be constructed in a cheap and reliable manner to be commercially viable. Many concepts have been proposed to meet these challenges over the years, with a wide spread in both form and function of the device.

1.1.1 Historical development

The idea to utilize the energy of ocean waves to power human technology can be traced back as far as 1799. Ross [137] describes the first patent on wave energy, submitted in Paris by Girard (father and son), as a floating pontoon connected through a lever to an onshore pumping station. However, the wave energy industry as it looks today, started for real during the oil crisis of the 1970's. Some key inventions were proposed and tested during this period which are still defining for classes of WECs today:

Salter cam Stephen Salter presented his idea of a drop-shaped cam (commonly known as the ”nodding duck”) pitching in the waves in 1973 [141] and it became the starting point for wave energy research in Europe [57]. The ducks were to be placed along a line with a shared axis, forming the original *terminator* type device. See figure 1.1(a).

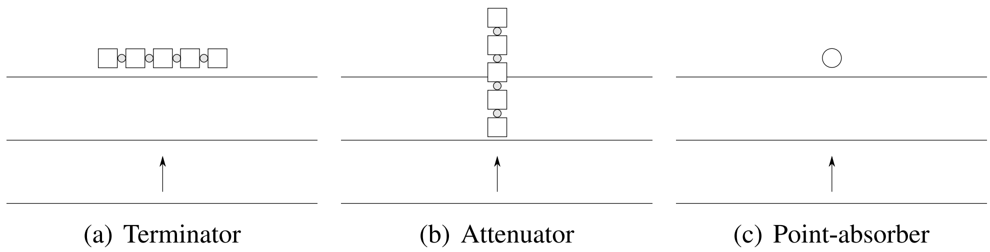

Figure 1.1: Classification of WECs by arrangement. The arrow indicates the direction of wave propagation, with wave crests shown as horizontal lines.

The oscillating water column, (OWC) The device type was invented by Yoshio Masuda already in the 1940's, but it was developed as an OWC in the UK during the 1970's [137]. A chamber of air is mounted in the water so that the water surface inside it is repeatedly elevated and lowered by the action of the waves. The oscillating air-pressure inside the chamber is used to drive an air-turbine that connects the chamber with the surrounding air through an orifice, as illustrated in figure 1.2(a). The chamber structure is ideally kept stationary during operation.

The Cockerel raft Invented in 1976 by sir Christopher Cockerel (also the inventor of the hovercraft). The original Cockerel raft had three hinged pontoons, and is considered to be the first *attenuator* type device [137], see figure 1.1(b). Hydraulic damping at the hinges between each pontoon were used to extract energy from the motion.

The point absorber Budal and Falnes [26] introduced the point-absorber concept in wave energy by studying small bodies that undergo large motions. They further developed extensive theoretical predictions on phase control and maximum power output [27] from this type of WECs. During this period in Sweden, research on similar point-absorbing concepts (the IPS buoy and the Hose pump) was made here at Chalmers University of Technology [16].

Overtopping The tapered channel was built in Norway in 1985, invented by a group at the centre for industrial research in Norway. The 350kW, shore-based TAPCHAN was the first overtopping type device [23]. Overtopping devices essentially allow the waves to spill into a basin of water. The mean water level inside is thereby increased, and the potential difference to the surrounding mean water level is used to drive low head hydro-turbines, see figure 1.2(b).

The theoretical work on the radiation and diffraction potentials applied to wave energy conversion by Newman [107], Evans [55] and Mei [104], aided to further increase the understanding of wave-structure interaction problems and was very

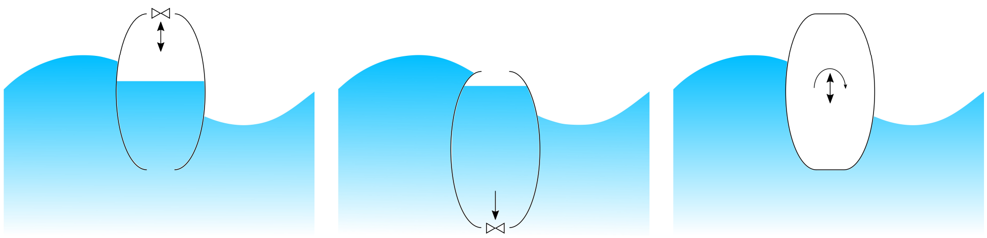

(a) OWC (b) Overtopping (c) Wave activated body

Figure 1.2: Working principle of three classes of WECs. (a) OWC, Oscillating Water Column (b) Overtopping and (c) Wave activated body.

important for the development of the WEC concepts. In the beginning of the 1980's however, the oil became affordable once again, and the financial support for these pioneering wave energy projects was drastically cut short [57].

1.1.2 A new generation

A second generation of wave energy concepts started to gather momentum and financial support from the turn of the millennium, as a response to the global awareness of the environmental consequences of a fossil-based economy [57]. A multitude of devices have since been proposed, and to date the European Marine Energy Centre (EMEC) lists over 200 developers of wave energy converting concepts [49].

Categorising WECs is almost a research area of its own. Different categories have been promoted based on shape, size, location, working principle, number of bodies and mode of motion [23, 56, 75]. Here we follow Hagerman [75] where a WEC is categorised by two labels, the interaction with the waves and the working principle. The interaction with the incoming wave relates to the shape of the device. Figure 1.1 shows the three main categories of WEC shape: (a) *terminators*, long structures aligned transverse to the wave direction, forming an artificial coastline to the wave; (b) *attenuators*, long structures aligned along the direction of propagation of the wave; and (c) *point-absorbers*, buoy-like structures which are small in relation to the wave length, acting like antennas in the wave field. The working principle label has instead to do with the means by which power is generated. The most common working principles are also conveniently divided into three categories depicted in figure 1.2: (a) *OWC*, the wave action drives an oscillating air-flow through a top-end turbine; (b) *overtopping*, waves spill over into a reservoir where the returning flow is used to power low-head turbines; and (c) *wave activated body*, the motion response to wave action is the driving force for energy extraction.

In Sweden, technology development has more or less converged to the point-absorbing, wave-activated body type of WEC, with three main developers: (i) *Waves4Power*, adopted from the IPS concept with hydraulic power take off [165];

(ii) *Seabased*, with a bottom-mounted, direct-driven linear generator [145]; and (iii) *CorPower*, with a rack-pinion drive and a novel passive control technology, see Hals et al. [76].

For more information on the current wave energy status of devices and types of WECs, see e.g. [40, 3, 56]. It should be noted that these references, and many other compilations of current WEC technology, include concepts that are no longer being developed. Notably, this applies to three front-runners of wave energy devices: the Pelamis (of attenuator type) [151]; the Wavebob (a two-body point-absorber) [22]; and the Oyster (bottom-mounted, hinged terminator) [14]. The failures of these enterprises were very bad for the reputation of wave energy as a possible source of energy, but they have also served to highlight the importance of a good and above all cost-efficient roadmap to full commercialisation of WEC concepts.

1.2 Motivation

1.2.1 Design considerations

So how to achieve a good design of a WEC concept? To answer this we must first understand the dual role that wave loads play in WEC design. On the one hand, the WEC hull and moorings must be designed to withstand the loads acting on them. On the other hand, the same loads are the driving force for power production, which by extension provides income to the project. So in a conservative cost versus revenue design loop, the loading on the structure should be overestimated for the structural integrity but underestimated for predictions of power production. Put together it means that wave energy developers have twice to gain on improving the accuracy of wave load estimation tools.

From a techno-economic perspective, a preferable rule-of-thumb in WEC design is to make sensitivity studies and design modifications as early as possible in the development. Such a design route was formalised by Weber [166] as a design matrix of technology readiness level (TRL, defined for WECs in [63]), versus technology performance level (TPL). The TPL scale is tied to the levelised cost of energy of a concept. High performance levels give cheaper electricity, and vice versa. The TRL measure is more associated with milestones such as e.g. prototype field tests, being grid connected, etc. Weber argues that considerable design changes in later stages of TRL are increasingly costly and that prototype testing should be done on a nearly optimal design. A diagram showing a preferable design path is shown in figure 1.3. In short, it is beneficial to increase TPL at a low TRL compared with changing the design for optimal performance at a later stage of development.

But which methods to use to achieve such a good performance in an early stage has not been discussed to the same detail. Pecher and Castillo [129] have compiled WEC development into five stages, based on the level of tests and experiments:

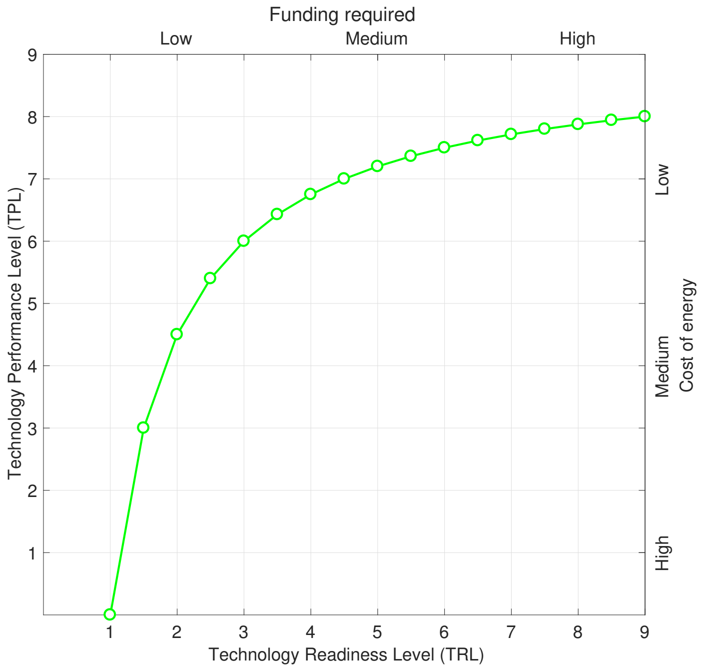

Figure 1.3: Preferable development path of a WEC, indicating performance before readiness. Illustration based on information in [129].

Concept model Laboratory experiments where most optimisation is made.

Design model Laboratory testing and adjustment of final design.

Functional model Laboratory or benign site test of real, small-scale device.

WEC prototype A single full-scale condition device.

Array demonstration Full-scale conditions of several devices.

The main optimisation of the device is concentrated in the concept and design stages, but numerical tools are in [129] confined to so-called wave-to-wire simulations in the design and functional model stages. Wave-to-wire models are computationally efficient tools that enable time-domain simulation of WEC response with the aim to estimate long term power production in a fraction of real time. They are generally based on linear potential flow theory, with body motions computed through the impulse response function due to Cummins [41], and constant coefficients from a radiation-diffraction pre-processor. The radiation-diffraction problem is typically solved by a boundary element method, like in WAMIT [164] or Nemoh [10]. For mildly non-linear cases, correction terms include parametrised drag forces [20], and non-linear Froud-Krylov forces [94].

Several researchers agree that wave-to-wire models can, and perhaps should, be used also in the earliest stages of development [44] to gain more understanding of the sensitivity of the design. Efficient numerical tools makes it possible to evaluate design iterations more extensively than using experiments alone. Wave-to-wire models are well-established in the wave energy sector and should be considered as the most common tool of the trade.

But it is one thing to do a basic evaluation of a design iteration. Another to evaluate one that shows promise in more detail and for a larger scale deployment. The difference comes down to accuracy and completeness of the modelling approach. The accuracy of wave-to-wire models is questionable for cases where non-linear effects are more important. For such cases, the use of so-called *high-fidelity* models becomes favourable. In high-fidelity models, computational fluid dynamics (CFD) is used to model the fully nonlinear problem of floating WEC response in waves.

If high-fidelity models become more involved in WEC design, the understanding of non-linear phenomena and design forces can increase and their effects can be better accounted for when producing the experimental models, prototypes and demonstration installations. We argue that an optimal TRL-TPL development route can be achieved most effectively by an underlying iteration between numerical and physical model tests, with more emphasis given to high-fidelity numerical models than what has previously been suggested.

1.2.2 Mooring challenges

The moorings are a key component in the technical feasibility of wave power projects. In fact, the international renewable energy agency (IRENA), lists cost-effective durable moorings/foundations as one of six prioritised areas of technology improvement for the wave energy industry [3].

Moorings of a wave energy converter need to comply with the same demands as other offshore structures. A permanently installed structure (25 year expected life-time) in e.g. the North Sea should be designed to survive the maximum wave expected in 100 years, which corresponds to waves more than 20 m high in places [46]. WECs are typically installed in water depths of < 100 m [40], so the design wave height is potentially a substantial part of the water depth. To this we must add the loads from ocean currents and tidal variations at the installation site. Clearly a moored WEC will under such extreme events be subject to very large influences from the waves. The moorings will either need enough flexibility to endure large displacements, or have enough strength to withstand the hydrodynamic loads while restraining the structural motion. The task of designing the best mooring can then be reduced to finding the best compromise between compliance and material strength for the design load cases. In addition to the station keeping functionality, moorings play an intricate role in the design of many WECs as they influence the hydrodynamic response amplitude. The mooring design is therefore closely linked to the power production efficiency [60], which is why moorings should be accounted for in a very early stage of WEC concept design and development. Mooring design considerations will be discussed in greater detail in chapter 3.

The rough offshore environment is still a challenge for mooring design also in mature businesses such as the oil and gas industry. Reviews of mooring line failures show that the majority of failures are in the first ten years of operation, with the bulk of failures occurring during the first five years [101, 102]. Another review of mooring incidents [140], focusing on the Norwegian continental shelf between 2000 and 2013, shows that 54% of the 26 maritime incidents investigated were due to mooring line breakage. The report goes on to list the most common technical causes of the cable failures:

- Excess loads on lines due to dynamic snap loads or unexpected weather conditions,
- Fatigue fractures in chains,
- Damage to fibre lines.

Focusing on the snap loads, they occur in cables for several reasons, as will be discussed in section 3.3. They are however most commonly associated with cable slack and the sudden snap that occurs when the cable is retightened. There are reports of snap loads causing damage also in wave energy field tests [78, 143]. In the current standard, DNV-GL [46] recommend that slack-snap conditions are avoided or kept below a minimum probability of occurrence. We argue that such a conservative design route needs to be re-evaluated for wave energy applications, where the expected dynamic range of the hull motion response is higher than in conventional structures such as ships or platforms. An alternative approach is to treat snap loads as any other load, but evaluate them with tools that correctly predict their occurrence, magnitude and duration of the snap. To be able to predict and mitigate the snap loads in the design iteration procedure would be very beneficial in the search for an optimal mooring system for WECs.

1.3 Aim

The work in this thesis aims to increase the accuracy of numerical models of WECs. Our primary focus is on mooring dynamics, where we aim to prove that high-order discontinuous Galerkin finite element methods can model mooring cables correctly and efficiently. The cable model developed in this thesis is particularly aimed at increasing the accuracy of snap load events in mooring cable modelling. For wave energy applications, we aim to show the importance of correct modelling of nonlinear effects on the WEC response, which also covers the restraining action of the moorings. This aim is focused on the demonstration of coupled CFD-mooring analysis for WECs and its potential importance in design iterations for WEC concepts.

The experimental work in Paper III was motivated by two main aims. It was indeed purposed to provide suitable data for validation of the coupled CFD model, but the main aim of the experiments was to investigate the influence of different mooring system designs in terms of their suitability for WECs.

1.4 Scope

We will focus on coupled, fully non-linear and viscous models of the moored motion of point-absorbing devices. The work can be divided into two parts, starting with the dynamic response of the mooring cables themselves. The main original contribution presented here is the development of a finite element model for mooring cable dynamics (Moody). The model is specifically designed for snap load events. It thereby complements available tools for mooring design and enables improved estimations of the maximum loads on the system. The model can also be used to improve the accuracy of fatigue life estimations on mooring components.

Two generations of Moody are presented. The first (from Paper I) presents the discontinuous Galerkin method as a way to model the motion of mooring cables, while the second (from Paper V) provides a better framework for shock capturing, i.e. snap loads. Results and computational examples are limited to verification and validation of the formulations and the numerical implementation. Due to time limitations, extensive benchmark studies against other software for cable dynamics and applications in field tests of actual devices are both considered to be outside the scope of this thesis.

The second part of the work concerns numerical modelling of moored floating structures in the resonance region. Hydrodynamic modelling of moored point-absorbers are made with transient Reynolds Averaged Navier-Stokes (RANS) simulations using the Volume of Fluid (VOF) method, see Papers II and IV. The simulations presented in this work are made with the OpenFOAM platform [110], adopted from [167]. A realistic moored motion is achieved by an integrated coupling to Moody simulations. The coupled method has very few underlying assumptions when it comes to the physical factors it takes into account, but the model complexity is also very much increased compared to more commonly used wave-to-wire models. The original contribution is here the implementation of the coupling and its ability to model a realistic restoring stiffness to the moving WEC. The completeness of the coupled model makes it suitable as a tool to study extreme events such as slamming loads or breaking waves. However, this work has focused on the nonlinearities of the resonance region, including viscous effects, but limited to mildly nonlinear, regular waves. Irregular waves have been regarded as too computationally intensive to manage within the scope of this thesis.

VOF-RANS simulations incorporate many numerical methods and schemes, e.g. turbulence modelling, free-surface capturing, wave generation and aborption and fluid interaction with the floating rigid body. Although touched upon in some of the discussions, the sensitivity of the results are not evaluated with respect to all of the settings used to model these phenomena. We especially mention that the turbulence model used throughout the thesis has been the RNG $k-\varepsilon$ model [173], and the sensitivity of the results towards other turbulence models are not presented or discussed herein. The local flow characteristics surrounding the body are only briefly commented in Paper IV. In general, the results are not discussed in terms of flow separation and the detailed discussion on the turbulent quantities of the near-body flow is left for future work.

1.5 Structure of the thesis

As previously mentioned, the thesis can be divided in two parts. In what follows, we begin with the theoretical framework for floating WEC dynamics. We explain the background and features of the CFD model used in papers II and IV, and provide a literature review of high-fidelity modelling of WECs, see chapter 2. Chapter 3 then focuses on mooring cable dynamics and begins with a more elaborate discussion and literature review on mooring design for WECs. Next a derivation of the governing equations for cable dynamics in marine applications is presented, and chapter 3 ends with a description of snap loads and a review of numerical models for cable dynamics. The theoretical background is finalised by chapter 4 where a review and short introduction to the discontinuous Galerkin method and its hallmark properties are given. The thesis is based on five appended publications, with contents summarised in chapter 5. The results and their engineering implications are discussed in chapter 6, and the conclusions are summarised in chapter 7.

2

Hydrodynamic modelling of WECs

This chapter elaborates on methods used to compute the motion of floating wave energy converters (WECs). The CFD method used in this thesis is described, and its differences compared with standard wave-to-wire models is highlighted. A literature review of previous work on CFD for WECs is also presented. However, we begin with some basic properties of water waves.

2.1 Water waves

The theory behind the spectral content of water waves is well developed and there is a vast literature on the topic. For good introductions to understanding the ocean environment and wave loads on offshore structures, consider the books by Dean and Dalrymple [45], Faltinsen [58] and/or Chakrabarti [29]. Here we will only describe some basic definitions of water waves, to support the discussion later. In particular, we will highlight the steepness dependence of the wave profile as an example of a nonlinear aspect of wave propagation.

A wave can be described by a set of connected parameters: the wave height H (m), the wave period T (s), and the wave length λ (m), see figure 2.1(a). The period and the length of the wave are directly corresponding to the wave frequency ω (rad/s) and the wave number k (rad/m) respectively as

$$\omega = \frac{2\pi}{T}, \qquad\qquad k = \frac{2\pi}{\lambda}.$$

Water waves are dispersive, i.e. different frequencies travel with different speeds. The parameters k and ω are related by the linear dispersion relation as

$$\omega^2 = kg \tanh kh, \tag{2.1}$$

where g is the earth acceleration and h is the water depth. T and λ are therefore linked, meaning that a wave is completely defined by either pair of (H,T) or (H,λ), provided that h is known.

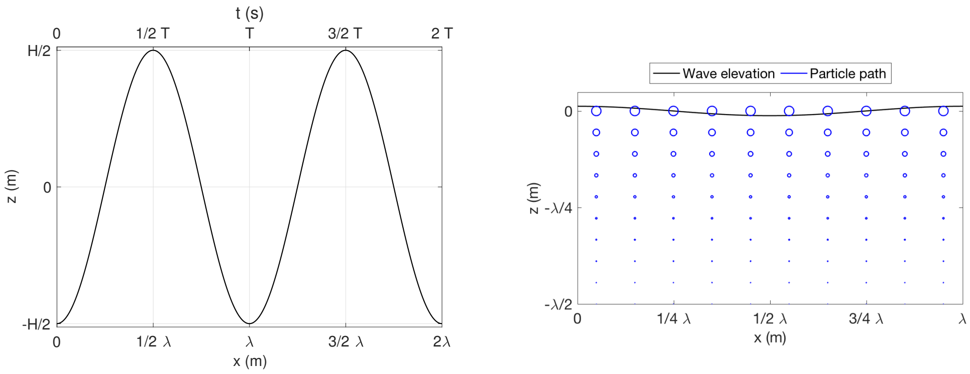

(a) Wave parameters (b) Particle paths

Figure 2.1: Basic properties of a linear wave. (a) shows the definitions of wave height H, wave length λ and wave period T. The upper axis is the time domain, and the lower axis is the spatial domain. (b) shows the circular paths of water particles in a linear deep water wave.

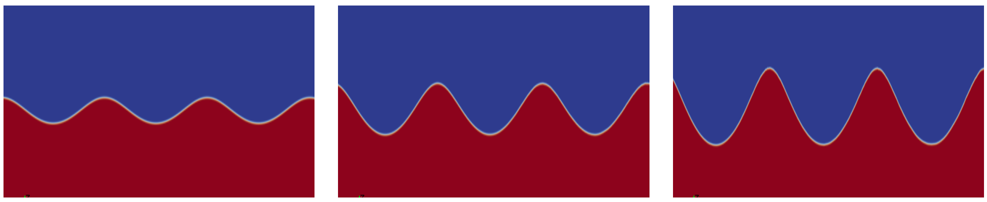

(a) $H/L = 2.5\%$ (b) $H/L = 5.0\%$ (c) $H/L = 7.5\%$

Figure 2.2: Steepness effect on the wave profile shown by a $T = 5\,\mathrm{s}$ wave with wave heights: (a) $H = 0.976\,\mathrm{m}$, $H/L = 2.5\,\%$; (b) $H = 1.952\,\mathrm{m}$, $H/L = 5\,\%$; and (c) $H = 2.928\,\mathrm{m}$, $H/L = 7.5\,\%$. The vertical axis is amplified by a factor of 10. Please note that the steepness was approximated based on the linear wave length. The true wavelength is slightly longer for the steeper waves. The figure shows results from a two-dimensional simulation using aspect ratio 2 and a constant resolution of $dz = 0.05\,\mathrm{m}$ for all three cases.

Figure 2.1(b) shows particle paths of a small-amplitude deep water wave. The paths are circular for small amplitudes and water depths larger than half the wave length. The relation between wave height and wave length, H/λ, is referred to as the steepness of the wave, which is a measure of the level of nonlinearity in the wave. For very small waves, $H/L < 0.02$, a linear approximation is valid and the wave profile is purely sinusoidal. For steeper waves, higher-order terms become important and the wave profile is transformed into one with sharper crests and wider troughs. Figure 2.2 shows an example of how the profiles of fifth order Stokes waves change with the steepness of the wave.

2.2 METHOD OF CHOICE

When choosing a method to compute WEC response in waves there are several aspects to consider, pertaining to:

- how the hydrodynamic flow is modelled;
- how the free surface is approximated;
- how the waves are modelled;
- how the floating body interacts with the flow; and
- how restraint forces from power take off (PTO) and moorings are considered.

In this thesis, we have aimed to model WEC motion by a complete and computationally expensive approach. The flow is modelled by incompressible Reynolds averaged Navier-Stokes (RANS) simulations, with the free surface captured by the volume of fluid method (VOF). The floating body motion is solved by direct integration of fluid pressure and shear force on the body surface, with the additional restraints from moorings and power take-off considered as external forces on the rigid body solver.

2.2.1 VOF-RANS

To explain the RANS simplification, we begin with the incompressible Navier-Stokes equations (NSE)

$$\nabla \cdot \mathbf{u} = 0\,, \tag{2.2}$$

$$\frac{\partial \mathbf{u}}{\partial t} + (\mathbf{u} \cdot \nabla)\,\mathbf{u} = -\frac{1}{\rho}\nabla p + \nu\,(\nabla \cdot \nabla)\,\mathbf{u} + \mathbf{f}\,, \tag{2.3}$$

where fluid properties are denoted by: $\mathbf{u}$ – velocity, ρ – density, and ν – kinematic viscosity coefficient (dynamic viscosity over density). Further, $\mathbf{f}$ denotes external body forces, p is the pressure, and

$$\nabla = \left[\frac{\partial}{\partial x}, \frac{\partial}{\partial y}, \frac{\partial}{\partial z}\right]\,.$$

Eq. (2.2) is referred to as the continuity equation, and eq. (2.3) is referred to as the momentum equation. To solve the full NSEs using direct numerical simulations is considered too expensive for most applications. A more feasible level of accuracy is achieved through Reynolds averaging, where the flow quantities are approximated as the sum of a time-averaged mean flow and a fluctuating part,

$$\mathbf{u} = \bar{\mathbf{u}} + \mathbf{u}'\,,$$

which by extension leads to the RANS equations:

$$\begin{aligned} \nabla \bar{\mathbf{u}} &= 0\,, \\ \frac{\partial \bar{\mathbf{u}}}{\partial t} + (\bar{\mathbf{u}} \cdot \nabla)\,\bar{\mathbf{u}} &= -\frac{1}{\rho}\nabla \bar{p} + \nu\,(\nabla \cdot \nabla)\,\bar{\mathbf{u}} - \nabla \overline{\mathbf{u}' \otimes \mathbf{u}'} + \bar{\mathbf{f}}. \end{aligned} \tag{2.4}$$

Here the influence of turbulence is approximated by the Reynolds stress tensor, $\overline{\mathbf{u}' \otimes \mathbf{u}'}$. In our simulations, this term was approximated using the RNG$-k-\varepsilon$ turbulence model, an eddy viscosity model first proposed in [173].

The RANS equations are solved using a cell-centered finite volume (FV) method, implemented in OpenFOAM [110]. The free surface is approximated through the volume of fluid method (VOF) where the two-phase problem of air and water is treated with a single fluid approach by the addition of a phase fraction parameter. The phase fraction, α, is used to indicate the mixture between air ($\alpha = 0$) and water ($\alpha = 1$) in each computational cell. The properties of density, ρ, and viscosity, ν, in eq. (2.4) are then computed from

$$\begin{aligned} \rho &= \alpha \rho_w + (1-\alpha)\,\rho_a\,, \\ \nu &= \alpha \nu_w + (1-\alpha)\,\nu_a\,, \end{aligned} \tag{2.5}$$

where index w and a indicate water and air respectively. At the free surface, high-gradients of α are limited using the SuperBee TVD limiter, discussed in e.g. [148]. In addition, the α-transport equation contains an artificial compression term which keeps the surface interface sharp, see [139] for a description of these VOF conditions. The VOF method is mass conservative and contains no assumption of the shape of the free surface. This is an important feature for the purpose of using VOF-RANS in wave energy applications because the method supports waves that overtop the WEC structure, as well as waves that are at the breaking limit of steepness. Although supported by the VOF as such, the accurate modelling of breaking waves is a difficult task. Turbulent effects become important to model the energy dissipation in the breaking [98]. Therefore, this work is limited to moderately nonlinear waves, and breaking waves are left to future studies using the VOF-RANS method applied to WECs.

2.2.2 Floating bodies

To complete our VOF-RANS model for WECs we need to solve also for the rigid body motion of the WEC structure. For floating bodies, it is customary to define a body-fixed coordinate system. Definitions differ in terms of placing the origin, but in this work we will use the centre of gravity of the body as point of origin. This is a logical choice for VOF-RANS models, as there is no explicit need to identify the wetted surface of the WEC hull. The WEC motion is simply the result of fluid forces from both fluid phases, although clearly dominated by the hydrodynamic contribution. Motion along the coordinate directions are labelled surge, sway and

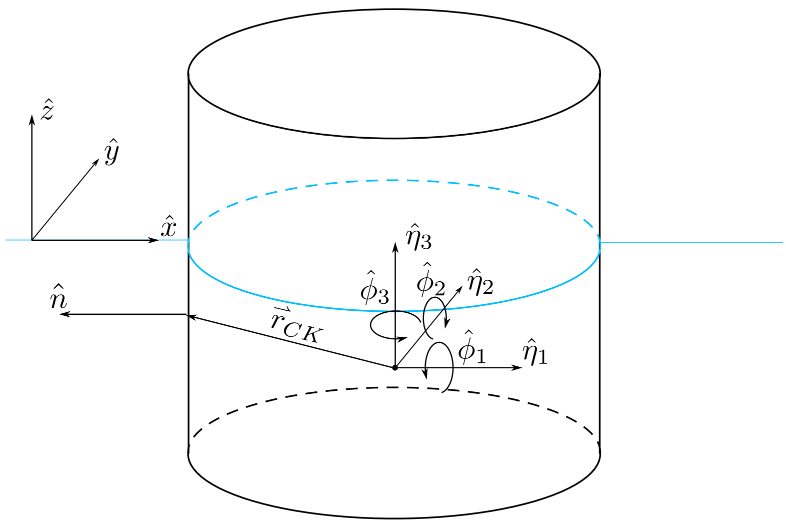

Figure 2.3: The coordinate systems of a floating rigid body. $\hat{\eta}_1$ is surge, $\hat{\eta}_2$ is sway, $\hat{\eta}_3$ is heave, $\hat{\phi}_1$ is roll, $\hat{\phi}_2$ is pitch and $\hat{\phi}_3$ is yaw.

heave, with corresponding rotations roll, pitch and yaw respectively. These six degrees of freedom are displayed in figure 2.3.

The balance equations of forces and moments on the body are

$$m_b \ddot{\vec{\eta}} = \int_K \vec{\tau} - p\hat{n}\,\mathrm{d}K + \vec{F}_{\mathrm{PTO}} + \vec{F}_{\mathrm{M}}\,, \tag{2.6}$$

$$I_b \ddot{\vec{\phi}} = \int_K \vec{r_{CK}} \times \left(\vec{\tau} - p\hat{n}\right)\mathrm{d}K + \vec{M}_{\mathrm{PTO}} + \vec{M}_{\mathrm{M}}\,, \tag{2.7}$$

where K is the entire surface of the body, m_b and I_b are the body mass and moment of inertia respectively, $\vec{\eta} = [\eta_1, \eta_2, \eta_3]$ is the position vector of the gravity centre and $\vec{\phi} = [\phi_1, \phi_2, \phi_3]$ is the vector of rotations of the local coordinate system. Further p and $\vec{\tau}$ are the fluid pressure and shear force on the body surface at a point with outward-pointing normal $\hat{n}$ and position vector $\vec{r_{CK}}$ relative to the centre of gravity. Finally, $\vec{F}_{\mathrm{PTO}}$ and $\vec{F}_{\mathrm{M}}$ represent the power take off force and the restraining action of the moorings on the body, with corresponding moment contributions denoted by $\vec{M}_{\mathrm{PTO}}$ and $\vec{M}_{\mathrm{M}}$ respectively. In the results presented in Paper II, the power take off was a constant coefficient linear damper for each mode of motion. The mooring force is computed for each time step in Moody, and returned to the rigid body solver. The interface between the mooring code and the rigid body solver is explained in more detail in chapter 5.

2.3 VOF-RANS versus wave-to-wire models

In summary, the VOF-RANS method is an advanced method with few underlying assumptions governing the flow. To put it in perspective with the previously mentioned wave-to-wire models, an overview of the differences between the two modelling approaches is given in table 2.1. Wave-to-wire models are aimed at producing estimates of power production, which puts high demands on the computational speed. VOF-RANS models are undoubtedly orders of magnitude more expensive than wave-to-wire models in terms of computational effort needed. However, the problem with using faster models only, is that it is difficult to pin-point exactly where the range of validity ends, and consequently which scenarios that result in uncertain estimations of WEC performance. We highlight that the VOF-RANS approach is sufficiently complete to model all kinds of highly nonlinear effects, such as extreme waves and large-amplitude motion with high accuracy. VOF-RANS simulations can therefore complement wave-to-wire models to quantify more of the nonlinear effects on WECs.

Table 2.1: Conceptual differences between VOF-RANS models and wave-to-wire models. * The non-linear Froude-Krylov forces and instantaneous wetted surface are here regarded as weakly non-linear corrections to wave-to-wire models.

Property	**Wave-to-wire**	**VOF-RANS**
Waves	linear	fully nonlinear
Overtopping	no	yes
Nonlinear response	weakly*	fully nonlinear
Radiation-diffraction	linear	implicitly included
Viscous effects	parametrised drag	turbulence model
Mooring	external force	external force
PTO	external force	external force
Comp. speed	very fast	very slow

2.4 Review of high-fidelity WEC models

There is a large body of work done on hydrodynamic WEC modelling. Li and Yu [97], Wolgamot and Fitzgerald [172] and even more recently the book by Folley [65] all provide very good overviews of both state-of-the-art and more advanced, fully nonlinear numerical models of WECs. The present review focuses on the widely used wave-to-wire models and on the high-fidelity approach with VOF-RANS. In between these methods there is a hierarchy of flow models which model part of the nonlinear effects for WECs. Here we will focus on the use of VOF-RANS and refer to [172] and the references therein for more information of the whole range of non-linear methods used for WECs.

State-of-the-art

The most common method of choice is wave-to-wire models based on linear potential theory and the radiation-diffraction method. In linearised form, they can be used in frequency-domain, but most recent efforts suggest time-domain wave-to-wire simulations to be state-of-the-art for WEC models [44]. In what follows, we will refer to time-domain simulations when we use the wave-to-wire label. Their popularity is due to their computational efficiency and good accuracy for many load cases, resulting in efficient estimation of annual power production. Nonlinear source terms from e.g. the power take off and the mooring system are easily included, while keeping the wave-exciting terms and the inertial contribution linear. The same approach is used by standard engineering tools, see e.g. [7, 48, 70]. In e.g. [11], wave-to-wire models have been used to benchmark performance of several different WEC concepts. The inclusion of non-linear Froude-Krylov forces can further increase the range of validity for wave-to-wire models, see Alves (ch. 10) in [129]. However, during large amplitude motions far from the equilibrium position, or when the dynamics of the wave become increasingly non-linear, the radiation-diffraction method is no longer valid and more advanced tools are needed [130].

Following the performance increase and availability of high performance computing, the use of VOF-RANS has grown rapidly in marine applications during the last ten years. It is now a well-trusted tool for complicated flow problems in ship hydrodynamics [93], and VOF-RANS simulations are also beginning to decrease the need for physical experiments in offshore oil and gas platform design [89].

Making waves

Wave loading is a key part of VOF-RANS models of wave energy devices. In their review of methods for extreme WEC loading, Coe and Neary [38] highlight the importance to treat specially the temporal and spatial discretisation of the waves:

> ”If a comparison of experimental data and CFD predictions for device response is planned, a separate validation to assess the accuracy of the waves in the numerical simulation can rule out a potentially large source or error.”

Here we highlight the work of Li and Lin [96] who studied wave loads on submerged and surface-piercing structures focusing on differences between regular and irregular wave loading . The non-linearities of the wave loading force on a vertical cylinder was modeled using OpenFOAM by Chen et al. [30]. Results were in good agreement with experimental data and deviations of up to 50 % on the wave loads from linear potential theory were noted. Moctar et al. found a 25% deviation between Morison formulae loads and CFD analysis for a jack-up oil-rig on three supports under freak wave loads.

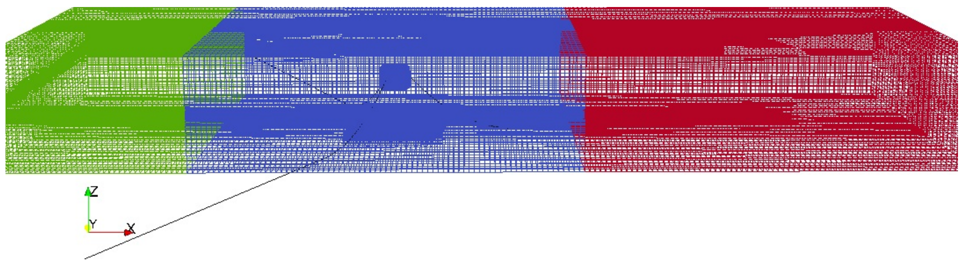

Figure 2.4: Overview of mesh regions used for generation (green), and absorption (red). The blue region is the undisturbed computational domain. From Paper IV.

Chen et al. [30] used relaxation zones for wave generation and absorption. Relaxation zones are essentially sponge zones of added numerical forcing to either dampen (absorb) the wave, or generate it. Typical zone sizes needed for a good absorption, i.e. with sufficiently low reflection, are two wave lengths [51]. Relaxation zones have been impemented in the popular waves2Foam package from Jacobsen et al. [85], which was used in papers II and IV. The main draw-back of the method is the added computational domain size needed just for the secondary task of generating appropriate boundary conditions. Figure 2.4 from Paper IV shows how a substantial part of the mesh is dedicated to wave generation and absorption.

An alternative approach is to run a potential solver in the background, and use it as boundary conditions for a body-centered CFD domain. In effect, the VOF-RANS model is then used for the body interaction with the waves only, while the far-field effects are approximated with potential flow. An example of this was shown by Paulsen et al. [128] who blended VOF-RANS with the OceanWave3D solver for fully nonlinear potential flow by Ensig-Karup and co-workers [50]. The result is a more efficient domain decomposition of the problem than when relaxing to analytical wave expressions, but buffer zones between the solvers are still needed.

A third option is to generate the boundary conditions directly at the domain boundary. This approach is called active absorption and is based on actively changing the boundary condition to generate a perfectly cancelling reflected wave. It is commonly used in physical model testing [67], and a numerical version was first implemented in a VOF-RANS solver in [157]. Later Higuera et al. [81] implemented a similar formulation in OpenFOAM based on the shallow water equations. They showed promising results and a significant speed up potential for engineering use of CFD models, compared to using relaxation zones. However, it is not possible to fine-tune the reflection coefficient as easy as in the relaxation/blending approach, where simply a larger zone or a better tuned damping coefficient can be used to achieve better results, albeit at a higher computational cost.

Device modelling using CFD

CFD simulations have been used to study oscillating water column type devices, e.g. [5, 84], oscillating wave surge type converters like in [144], and overtopping devices like in [54]. All in good agreement with experimental data. For a deeper insight into nonlinear models applied to WECs of all types, see [134]. For a review of the use of OpenFOAM in particular, see [42].

For wave energy devices of point-absorbing type, early work on CFD with VOF-RANS is due to Agamloh et al. [1], already in 2008. Agamloh and co-authors developed a coupled rigid body solver to a commercial code and used it to study both one and two truncated cylinders in regular and irregular waves. The cylinders were moving in heave only. Results indicate that the efficiency of absorbed power for a given frequency is reduced when the wave height increases. This was also shown in the experiments and VOF-RANS simulations of Yu and Li [177] in 2013, where the heave motion of a two-body converter was studied. They showed a significant reduction in power capturing efficiency when the wave height increased. However, the CFD simulations were underpredicting the experimental results as the steepness increased. The device had a low free-board that caused overtopping in steeper waves. This complicated the interpretation of the underlying causes of the power capture reduction. Our Paper II [118] was also presented in 2013 and showed the same type of efficiency reduction. Simulations were made in full scale, in six degrees of freedom with and without PTO and dynamic moorings. Results were compared with linear theory from Fitzgerald [62], who designed the generic WEC. Yu and co-authors [178] have more recently studied WECs using Monte-Carlo simulations of a wave-to-wire model to pin-point extreme events from the stochastic wave load scenarios. Deterministic simulations of these events where then analysed using CFD .

Coupled CFD-mooring simulations were first achieved in 2003, by Aliabadi [4]. They coupled a dynamic system of discrete masses (much like the OrcaFlex mooring solver [111]) to the motion of a moored floating barge in waves. Yu and Li [176] presented moored simulations using linear springs to represent the mooring restraint, as did Anbarsooz et al. [6] for the Bristol cylinder. Both studies present good correlation with experiments. Nichols-Lee et al. [108] also presented a coupling between two commercial solvers to establish a similar approach as in Paper II for a floating barge-like converter. For simulations in three degrees of freedom, they concluded that the completeness of coupled RANS-mooring simulations was needed to achieve reasonable results of moored response. The exact nature of the coupling is not described in the paper. Commercial codes for CFD analysis have in later years included couplings to dynamic mooring codes, see e.g. [64], and coupled methods can now be labelled state-of-the-art in CFD-mooring analysis. However, to date and to the authors knowledge, no mooring studies have yet been presented using these tools on moored wave energy converters.

Some work has also been done on using CFD to parametrise faster models for predicting WEC response. Bhinder et al. used CFD to define drag coefficients of a floating WEC in [20] and for a surging type device in [21], showing good agreement with experimental data. Davidson et al. also used CFD as input to a system identification framework to improve the non-linear performance of wave-to-wire models of generic point-absorbers [43].

The full nonlinearity of CFD simulations is utilized when applying control to the power capturing system of WECs. Giorgi and Ringwood showed that phase-controlling for optimal power output amplifies the nonlinearities beyond the scope of linear theory, even for a relatively mild wave steepness [69]. They concluded that not only do power output under control require CFD modelling for a conservative estimate of power production, CFD simulations are essential to obtain correct control variables for the control strategy.

3

Mooring dynamics

This chapter provides an overview of moorings of wave energy converters (WECs). We focus on the challenges of mooring WECs and present a short introduction to mooring properties in a simplified design. The interested reader is further referred to the mooring chapters in [129] and [47], and the work on mooring configurations by Fitzgerald [60]. The chapter continues with the governing equations of cable dynamics, a description of the physics behind snap load generation in moorings, and a literature review of numerical models for cables.

3.1 Mooring overview

Loads on a WEC can for the purpose of mooring design be divided into drift forces (also called low-frequency or slowly-varying forces) and wave-frequency loads. For large structures, far from resonant response, the slowly-varying loads are the primary design case for the mooring system as the wave-excited motions are limited. For smaller bodies designed to operate with large response however, wave-frequency loads are important for the mooring design. The moorings also affect the response of the device, which gives us a coupled problem [62]. For wave-activated body type WECs that aim to maximise their motion in the wave-frequency range, we would ideally like to have the mooring system working as a high-pass filter, restraining the slowly varying drift motion, but allowing free motion of the body in the wave-frequency range.

3.1.1 List of demands

Many configurations and materials have been proposed to achieve a good mooring for floating WECs. The list of demands on the moorings is however long and complicated, so this is not a simple task. The following is a summary of key design considerations for mooring systems of WECs (compiled primarily from Harris et al. [79], Harnois [78] and Fitzgerald [60]):

- The moorings must keep the device on station to a given tolerance. For WECs, this is generally decided by the distance to neighbouring devices in an array or the maximum offset allowed by the electric power cable.
- The moorings must remain intact under load requirements from classification guidelines, e.g. [46] under ultimate limite state (ULS), accident limit state (ALS) and fatigue limit state (FLS).
- Ideally, the moorings should provide sufficient compliance to minimise the loads on itself and the moored structure.
- In operational conditions, the moorings should not act detrimentally on the power absorption. If moorings are integrated in the design, this does not necessarily mean that the mooring stiffness should be minimised. It simply means that the mooring action must be included in the expected power production, and in designing the power take off mechanism.
- For array efficiency considerations, the horizontal footprint of the mooring should be minimised.
- Possible inter-moorings in arrays must enable the removal of an individual device for service and maintenance without affecting neighbouring devices.
- Marine growth, long term ageing and corrosion should be taken into account in the design.
- Slack-snap conditions should be avoided (or, as we will argue in the discussion, rigorously computed)
- The installation of the moorings should be made as easy as possible. This applies: (i) to the anchors used, which governs the size of ship needed; (ii) to the weight of the cables, where lighter is more manageable; and (iii) to the method used to prestrain the system.
- Inspection, maintenance and possible replacement of mooring components must be possible within a normal weather window.
- The mooring system as a whole has strong financial constraints and must be cheap in relation to the investment in each device.

Please note that this list is most applicable for WECs where a restraining action from the moorings is considered detrimental to the power capturing capability of the device. The multitude and diversity of WEC types makes truly generic lists too general.

3.1.2 Mooring materials

The slack-moored catenary chain is the classic image of a mooring system in marine applications and the most common choice of anchoring in shallow to medium depths. The increasing total weight of the lifted chain when the mooring attachment point (also called the fair-lead) is elevated provides a non-linear restoring force with a progressive stiffness [129]. For mooring point-absorbing WECs, the catenary mooring has a major draw-back. It takes up a large space on the seafloor (footprint), and in array installations the footprint for an efficient device placement must be small [60]. As an alternative, more elastic materials made of synthetic fibres are proposed, readily used in deep-water moorings of offshore installations. Weller et al. [168, 169] have made several investigations and experiments at the South West Mooring Test Facility, and have provided an insight in the suitability of nylon ropes for the mooring of WECs. They highlighted the long-term change in stiffness, the hysteretic effect in nylon lines, the effect of ageing, and the partial damage of marine growth as the primary problems. In [158] we find a nice overview of material properties of different synthetic fibres, see table 3.1. High-performing fibres (HMPE) such as Dyneema or Kevlar approach the stiffness of steel chains with break load elongation at 3-5 %, while nylon allows strains up to 30 %.

Table 3.1: Typical range of break load elongation of different fibre types. The numbers are primarily a subset of the full table in Tsukrov et al. [158], with the exception of the rubber-based mooring that refers to the Seaflex material [15].

Material	**Elongation at break load (%)**
HMPE	3-6
polypropylene	7-12
polyester	15-25
nylon	20-30
rubber-based	> 80

3.1.3 Previous studies

Without the weight of the chain, synthetic moorings are often combined with intermediate buoys (floaters) and clump-weights (sinkers). Early work on floaters was presented in [103] for deep water moorings of offshore structures. Later Krivtsov et al. [92] studied varying floater sizes and shapes for an experimental model of an OWC-WEC device. They concluded that soft moorings with larger floaters had smaller peak tensions near resonance, but for frequencies away from the resonant region of the device, stiffer moorings with smaller floaters appeared to lower the peak tensions. We also highlight the parametric studies of Fitzgerald [61], who showed dramatic changes between configurations in a numerical study of a reference load case on a generic point-absorber. The catenary mooring design was subjected to repeated slack-snap events resulting in very high peak loads, while designs with floaters overall had a smaller dynamic tension range. Other work on moorings for WECs include Vicente's array simulations using inter-mooring chains to connect several devices directly. The moorings were in [162] considered quasi-static, but dynamic simulations (using Moody and Orcaflex [111]) are included in his thesis work [161]. We also highlight the extensive modelling and experimental work on moorings from Harnois et al. [78]. In comparing a surge-corrected numerical model (Orcaflex [111]) with tank tests of mixed chain and nylon configurations, they show good results and emphasise the importance of a good surge model for mooring validation purposes. They also compare with field tests where they show large differences between model scale and prototype scale measurements. This is one of the few field test validation efforts and it highlights the difficulty in comparing parametrised models with the uncontrolled environment at sea. Influence of more uncertain wave measurements and marine biofouling can then have large impact on the results. The effect of biofouling was also studied numerically by Yang [175], where simulations with DeepC [48] showed large differences in fatigue life estimation for cases with and without biofouling on the moorings of a point-absorbing WEC. A recent and interesting approach to mooring design for WECs was suggested by Ortiz et al. [112]. A method for modelling mooring uncertainty and optimisation of the design for power production was implemented through a meta-model, which enabled a large set of mooring configurations to be evaluated during the design iterations.

3.1.4 Configurations

In Paper III we consider three general configurations of moorings: (A) a synthetic rope with an intermediate floater; (B) a synthetic rope with the same floater and an additional sinker placed closer to the buoy; and (C) a catenary mooring. The configurations are placed in three mooring legs as in figure 3.1(a). We use a simple quasi-static analysis of these systems to explain the fundamentals of mooring design.

In figure 3.1(b) we see net horizontal force on the body from the action of the three mooring legs. The mooring force of the three mooring legs cancel in the equilibrium position, but for a horizontal offset δ, we get a net horizontal restoring force $F_x(\delta)$. As we see from the similar slopes of the graphs in figure 3.1(b), the configurations were designed to have a comparable horizontal stiffness at the equilibrium position. This was done to achieve similar surge offset per drift force, and thereby enable a more suitable performance evaluation of the designs relative to each-other. The drift force will offset the mooring response characteristic, which has a large influence on the device performance and on the maximum loads in the system. From the side view of the cables in (c)-(e) of figure 3.1, we no-

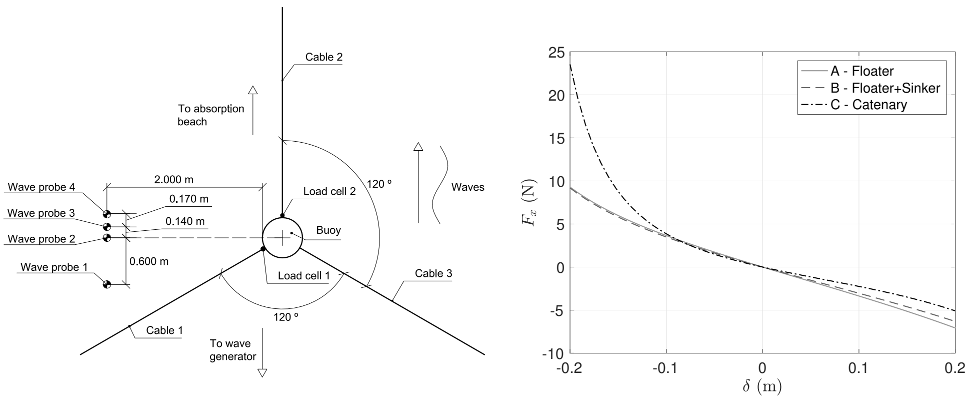

(a) Top view (b) Displacement-force

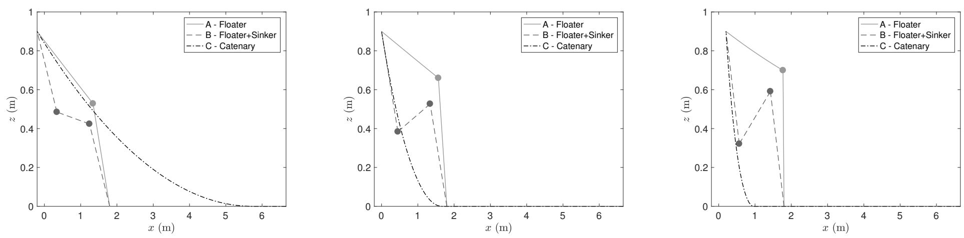

(c) $\delta = -0.2$ m (d) $\delta = 0$ m (e) $\delta = 0.2$ m

Figure 3.1: The layout and stiffness of the three configurations studied in Paper III. (a): Top view of mooring leg layout. (b): Horizontal displacement-force diagram. δ denotes an offset from the equilibrium along the wave direction shown in (a). F_x is the horizontal net force from all three legs. (c)-(e): Side view of the leeward mooring leg (cable 2 in (a)) for displacements δ =-0.2, 0, and 0.2 m respectively.

tice that a $\delta = \pm 0.2$ m displacement is approaching the maximum possible for the configurations. For $\delta = 0.2$ m, the near vertical lower line of configuration A in figure 3.1(e) indicates that the upper line is close to becoming slack. At the other extreme, figures 3.1(c) and 3.1(b) at $\delta = -0.2$m show how the stiffness of configuration C quickly grows as the the touch-down point approaches the anchor point of the catenary chain. This is further amplified by the fact that the leeward leg is perfectly aligned with the offset direction. From this first approach, it would seem that configuration B is the most robust to large, slowly varying displacements. However, as we will further discuss in Paper III, the complete answer is not so straight-forward when also the dynamic effects of the mooring cable response are taken into account.

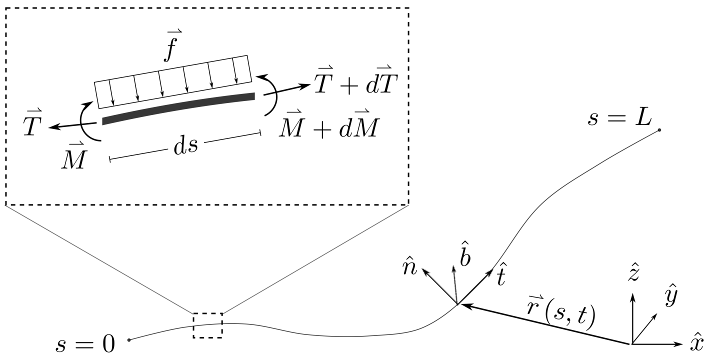

Figure 3.2: The coordinate systems of cable dynamics, including balance of forces acting on an infenitessimal piece of cable.

3.2 Cable dynamics

Let us now turn to the characteristics of cable dynamics, its governing equations and physical effects. A cable is a slender structure, i.e. its cross-sectional diameter is much smaller than the dominant length scale of the model problem. For marine applications typical length scales are the water depth, the floating structure width, the wave length of the dominant wave, or the length of the cable itself, against all of which the cable diameter is dwarfed. However, its cross-sectional parameters and properties are still important and need to be considered. The relation between the stiffness and the damping of the cable due to axial stretching, bending action or torsional deformation are important factors that govern the cable response. In this work, these properties will be regarded as part of a constitutive model and will not be studied in further detail. The reader interested in the particulars of constitutive modelling of cables is refered to the review by Spak and co-authors [146], which focused on model development for helically wounded wire-strand ropes.

The equations of motion of cables are well studied in a wide range of engineering applications. In the case of strings (no bending stiffness) a derivation was presented by Routh already in 1860 [138]. In what follows, we will give a short derivation of the equations of motion and show which assumptions that have been made during the cable model development presented in papers I and V.

3.2.1 Coordinate systems

Let us place a cable of length L in a global three-dimensional space, defined by the coordinate system (x, y, z) according to figure 3.2.

We define a one-dimensional local cable coordinate $s \in [0, L]$ directed along its centre line, mathematically referred to as a curvi-linear coordinate [105, 132]. At each value of s along the cable, the cable position vector can be expressed as

$$\vec{r}(s,t) = [r_x(s,t),\, r_y(s,t),\, r_z(s,t)]^{\mathrm{T}} \,.$$

The cable orientation is further denoted by its tangential vector (of unit length),

$$\hat{t} = \frac{\frac{\partial \vec{r}}{\partial s}}{\left|\frac{\partial \vec{r}}{\partial s}\right|}\,. \tag{3.1}$$

Worth to note is that many formulations use a local coordinate system to describe the cable equations. Some are fixed to the structure with one of the local axes aligned with the tangential vector, while the normal and bi-normal directions are fixed relative to the cross-section. This is most suitable for cross-sections with asymmetric properties. For axially symmetric cross-sections, a common choice of local frame is the Frenet frame. The Frenet frame also uses $\hat{t}$ as one axis, but defines the normal direction as the direction of the curvature of the cable, see e.g. the derivation of Tjavaras [152]. In the following analysis however, we follow the formulations of e.g. [99, 105, 132] and stay in the inertial frame to arrive at the equation of motion for a submerged cable in global coordinates.

3.2.2 Equation of motion

We study the single cable segment of length ds, located in the inertial frame. In figure 3.2 $\vec{T}$ is the internal force vector, $\vec{M}$ the internal moment vector and $\vec{f}$ represents the distributed external forces acting on the segment.

Figure 3.2 shows a segment of the cable along the unstretched cable coordinate s. As the cable domain stretches, the stretched length of the segment, ds', becomes

$$ds' = (1+\varepsilon)ds\,, \tag{3.2}$$

with the cable strain denoted by ε. For circular cross-sections with Poisson's ratio 0.5, the cross-sectional area A and diameter d in the stretched and unstretched domains are related to the strain by:

$$A'ds' = Ads\,,$$

so that

$$A' = \frac{A}{1+\varepsilon}\,, \tag{3.3}$$

$$d' = \frac{d}{\sqrt{1+\varepsilon}}\,. \tag{3.4}$$

The balance of forces in the stretched domain can be written:

$$\frac{\partial}{\partial t}\left(\gamma_0 \vec{v} ds'\right) = \vec{T} + d\vec{T} - \vec{T} + \vec{f}' ds'\,, \tag{3.5}$$

or, as per eq. (3.2) equivalently in the unstretched domain:

$$\frac{\partial}{\partial t}\left(\gamma_0 \vec{v} ds\right) = d\vec{T} + \vec{f} ds\,. \tag{3.6}$$

Here γ_0 represents the cable mass per meter with γ_0' being the stretched domain equivalent, and $\vec{v} = \frac{\partial \vec{r}}{\partial t}$ is the cable velocity vector. Division with the segment length ds, and letting $ds \to 0$, allows eq. (3.6) to be written as

$$\frac{\partial}{\partial t}\left(\gamma_0 \vec{v}\right) = \frac{\partial \vec{T}}{\partial s} + \vec{f}\,. \tag{3.7}$$

For a more complete derivation including bending stiffness for circular cross sections of negligible rotational inertia please see e.g. [152] and the references therein. The appended publications in this thesis are however based on the special case of no bending or torsional stiffness, which is true in the case of chains and a suitable approximation for most mooring cable materials in operation [47]. In the case without bending stiffness, the internal moment disappears ($\vec{M} = d\vec{M} = 0$ in figure 3.2) and the cable is unable to sustain shear forces. The tension force is therefore always tangential to the cable and eq. (3.7) is simplified to

$$\frac{\partial}{\partial t}\left(\gamma_0 \vec{v}\right) = \frac{\partial T\hat{t}}{\partial s} + \vec{f}, \tag{3.8}$$

where

$$T = \left|\vec{T}\right| = \sqrt{\vec{T}\cdot\vec{T}}, \tag{3.9}$$

is the tension force magnitude.

3.2.3 External forces

External forces acting on the cable arise from gravity and the pressure and shear forces of the surrounding fluid. As long as the mooring cable can be regarded as a slender structure, we can assume that the dynamic fluid variation across the cable cross-section is small and that Morisons formulae can be applied. Morison et al. [106] devised that the hydrodynamic forces acting on a small body can be split into buoyancy terms, drag terms in phase with the relative velocity, and inertial terms in phase with the relative acceleration. To describe the forces we first introduce the relative velocity and acceleration of the cable and the fluid as:

$$\vec{v}^* = \vec{v}_f - \vec{v}_c\,, \tag{3.10}$$

$$\vec{a}^* = \frac{\partial \vec{v}_f}{\partial t} - \frac{\partial \vec{v}_c}{\partial t}\,, \tag{3.11}$$

where $\vec{v}_c$ is the cable velocity and $\vec{v}_f$ is the fluid velocity. Naturally, these forces are very different if the cable is aligned to the relative flow or normal to it. To further keep notations short, we also specify

$$\vec{x}_{\hat{t}} = \vec{x} \cdot \hat{t}\,, \tag{3.12}$$
$$\vec{x}_{\hat{n}} = \vec{x} - \vec{x}_{\hat{t}}\,, \tag{3.13}$$

as the tangential and normal decompositions of a vector $\vec{x}$ respectively. Please note that subscript $\hat{n}$ according to eq. (3.13) is vector specific.

We can now split the external force f in eq. (3.7) into four terms:

$$\vec{f} = \vec{f}_A + \vec{f}_B + \vec{f}_C + \vec{f}_D\,, \tag{3.14}$$

each of which is briefly explained below.

$\vec{f}_A$: **Added mass forces** The acceleration of a (small) submerged body far from the free surface, experiences an added inertial force due to the mass of the surrounding water. We follow Morison and parametrise this by a constant coefficient C_M multiplied with the cable cross section area and the relative acceleration. $\vec{f}_A$ also include the Froude-Krylov force, estimated for small bodies as the body displacement multiplied by the external fluid acceleration. Denoting the fluid density by ρ_f, we can express $\vec{f}_A$ as

$$\vec{f}_A = A_c \rho_f \left(\dot{v}_f + C_{\mathrm{Mn}} \dot{v^*}_{\hat{n}} + C_{\mathrm{Mt}} \dot{v^*}_{\hat{t}} \right)\,. \tag{3.15}$$

$\vec{f}_B$: **Buoyancy and gravity.** The net force from buoyancy acting on the submerged cable can be described by the ratio of material densities between the materials. With ρ_c as the cable material density and g as the earth acceleration, $\vec{f}_B$ becomes

$$\vec{f}_B = \left[0,\, 0,\, -\gamma_0 g \frac{\rho_c - \rho_f}{\rho_c} \right]^{\mathrm{T}}\,. \tag{3.16}$$

$\vec{f}_C$: **Contact forces.** Cables are frequently subjected to problems of contact mechanics, including in lifting operations, around pulleys and during deployment from drums. Mooring cables, and in particular moorings of steel chain type, frequently interact with the sea-bed in what is called the touch-down region of the cable. $\vec{f}_C$ is in this work modelled as a bi-linear spring-damper, see papers I and V for details.

$\vec{f}_D$: **Drag forces.** The drag forces are in the Morison equation parametrised as proportional to the square of the relative velocity. The force is the vector sum of the normal and tangential contributions. The drag force is computed from

$$\vec{f}_D = d\sqrt{1+\varepsilon}\,\rho_f \left(C_{\mathrm{Dn}} |v^*_{\hat{n}}| v^*_{\hat{n}} + C_{\mathrm{Dt}} \left| v^*_{\hat{t}} \right| v^*_{\hat{t}} \right)\,. \tag{3.17}$$

3.2.4 Strain measures

Depending on the application, different approximations of the strain become prudent. We use the elongation of the centre-line coordinate, s, defined from the cable orientation vector as

$$\varepsilon = \sqrt{\frac{\partial r}{\partial s} \cdot \frac{\partial r}{\partial s}} - 1 \,. \tag{3.18}$$

Another common approach is the Green-Lagrange strain tensor. The axial elongation of the cable is then approximated by

$$\tilde{\varepsilon} = 0.5 \left(\frac{\partial r}{\partial s} \cdot \frac{\partial r}{\partial s} \right) - 1 \,. \tag{3.19}$$

To compare, the Green-Lagrange strain is a valid approximation up to 14% elongation (correct to 99%), after which the difference between the strains quickly grows. Green-Lagrange strain is often referred to as a large deformation strain measure, as opposed to the small strain approximation that requires strains below a few percent for good results. But when comparing with break-load strains in table 3.1, strain requirements are in some cases very high. To encompass all possible materials, we use the full definition in (3.18) to implement the mooring model in papers I and V.

3.3 SNAP LOADS

A snap load in a mooring cable can occur in several ways. The most common and intuitive reason for a snap load is that the mooring cable becomes slack (or almost slack) and then retightened. This can of course happen when the cable is subjected to very large end-point motions, in moorings most often in the leeward cable of a device experiencing substantial drift offset, e.g. figure 3.1(e). The snap magnitude is governed by the axial stiffness of the cable and the relative velocity of adjacent points at the moment the cable returns to tension [80]. Here we also mention the study on segmented cables by Goeller and Laura [74] showing the differences between response in dry and wet nylon, as well as the possible snap load mitigation of using shock-absorbing elements. The experiments of Fylling and Wold [68] and Suhara et al. [147] investigated snap loads by forced end-point motion tests concluding that the snap condition and the peak load are connected to the free-falling velocity of the submerged cable. Apart from the net force of buoyancy, the free-falling velocity is governed by the level of drag damping. In forced oscillation tests of a catenary chain mooring, Suhara et al. [147] classify the dynamic response in four categories.

Quasi-static response has no dynamic effects. This is evident for long-period motion.

Dynamic range is a response of sinusoidal appearance. Such harmonic results are seen at intermediate velocities.

Snap condition appears when the minimum tension force becomes zero and the cable is slack for periods of time. Snap loads appear, but the results are still periodic with respect to the end-point loading time period.

Free fall condition is entered when the transverse cable velocity exceeds the free-fall velocity of the cable. The resulting tension force is highly irregular.

Another type of snap load occurs in the touch-down region of catenary moorings. Gobat and Grosenbaugh verified by experiments and numerical predictions that a discontnuous force is generated when the cable touch down point moves faster than the transverse propagation speed [72]. This had been predicted by theoretical studies of Triantafyllou [154]. In [71] Gobat argued for the fatigue implications of this type of load in the touch-down region.

A third type of snap load is that which originate from a non-linear material response. For cables this was studied by Tjavaras [152] using the method of characteristics and finite differences to model the shock build up in cables with exponential strain-force dependence.

The challenges of modelling the occurrence and consequences of snap loads in mooring cables have been a large part of the motivation behind the work on numerical cable modelling presented herein.

3.4 Numerical models of cables

One of the first discrete models of non-linear cables was due to Walton and Polachek, who derived the relations of submerged cables in a finite difference setting already in 1959 [163]. Much work on oceanographic mooring has since been made, where the work of Triantafyllou and co-authors (e.g. [154, 155, 156]) is most noticeable. See also [47] for a good description of numerical mooring cable considerations and an overview of numerical models of cables. In 1999, Brown and Mavrakos [24] made a comprehensive benchmarking of different cable models. They showed that time domain simulations were needed for good accuracy and that frequency domain approaches and quasi-static simulations gave fundamentally different results for some cases. We especially point out the effect of mooring induced damping on the structural motion, which is not included in quasi-static analysis. The mooring damping can have substantial impact on the estimated motion of both floating platforms [100] and of WECs [86].

Some cable models are based on discrete masses connected with springs and dampers, such as [111], while some are based on linear finite elements, see e.g. [48, 7]. Valuable contributions to cable models using finite differences were made by Tjavaras [152] and Gobat [71]. Tjavaras developed robust formulations based on both Euler angles and Euler parameters for cables including bending stiffness. Gobat [71] later implemented the implicit generalised $\alpha-$method with adaptive time stepping to control the level of numerical diffusion in the system. The numerical predictions of the experimental tests showed good results.

For finite elements, some solvers use high-order elements. Buckham et al. [25] presented a cubic spline approach enforcing continuity of the cable position and orientation at each element boundary. We also highlight the work of Raknes et al. [132]. They use an iso-geometric mapping basis (NURBS) where the bending stiffness is included in a formulation using global coordinates and the Green-Lagrange strain approximation. Other formulations have used local coordinates to model the bending effect. Finally, and of special interest to the present contribution, there is the work of Montano et al. [105] who introduced mixed finite elements of arbitrary order in cable models. Montano allows the tension force to be discontinuous, but piecewise constant in each element. The formulation is in global coordinates under the assumption of negligible bending stiffness. The implementation is devoted to inextensible cables, and the tension force is applied as a multiplier constraint. In inextensible cables, the tension is instantaneously distributed along the cable, and longitudinal wave propagation is not feasible to model.

A numerical model that aims to compute snap loads with high accuracy will have two major restrictions. One is the time step size, which needs to be sufficiently small to support the propagation of longitudinal waves in the cable. We stress that this applies regardless of whether implicit or explicit schemes are used. Sharp tension gradients further require a numerical scheme that supports discontinuities and can capture these loads without numerical oscillation or instabilities. The purpose of papers I and V is to show that a high-order discontinuous Galerkin framework is a possible candidate to capture these loads with good accuracy and computational efficiency. The following chapter gives an introduction to the discontinuous Galerkin method.

4

The discontinuous Galerkin method

The discontinuous Galerkin method (DG) is conceptually a finite element (FE) formulation with strong links to finite volume (FV) methods. In principle the DG method is a FE formulation inside each element, while inter-element coupling is achieved through a numerical flux, as in the FV method. The inter-elemental flux is at the core of DG analysis, and different varieties of fluxes have been proposed to solve problems in a wide range of applications, for both fluid dynamics and structural mechanics.

This chapter describes the fundamentals of the DG method. It is assumed that the reader is familiar with the continuous Galerkin (CG) method used in finite element analysis. A short history of the DG family of methods is provided, followed by a derivation of the DG formulation for the linear advection equation with a Lax-Friedrich flux.

4.1 BACKGROUND

The DG method was introduced in 1973 by Reed and Hill within the field of Neutron transport problems [133]. However, the method picked up momentum first in the late 1980's and early 1990's when Cockburn and Shu developed the Runge-Kutta Discontinuous Galerkin (RKDG) methods in a series of publications [34, 32, 31, 33, 36]. The RKDG framework of methods was developed to solve non-linear hyperbolic conservation laws using explicit Runge-Kutta time stepping on a spatial discretisation using the DG method. It was originally developed as an improved method for advection dominated problems, as is well explained in Cockburn and Shu's comprehensive review from 2001 [37]. The RKDG method was extended to elliptic problems by Bassi and Rebay [12], which was later generalised by Cockburn and Shu's local discontinuous Galerkin (LDG) method [35]. An independent branch of discontinuous methods aimed at parabolic and elliptic equations is the interior penalty method (IP) by Arnold [8]. A unified analysis of

DG methods for elliptic problems, using both RKDG and IP, was proposed and discussed in [9].

The development of the DG method described above was mainly focused on problems in computational fluid dynamics. It has also been used for solid mechanics. A few examples are: problems of elasticity (a mixed formulation proposed in [77], extended to adaptivity in [83]), seismic wave propagation [88], and coupled elastic-acoustic wave propagation [171].

4.2 DG FOR A MODEL PROBLEM

The derivation of the DG formulation is very similar to the standard CG FEM as described in many text books, see e.g. [13]. This section aims to explain the main steps to get to a DG formulation from a model problem. We start with a scalar hyperbolic conservation law, namely the one-dimensional advection equation:

$$\frac{\partial u}{\partial t} + \frac{\partial F(u)}{\partial x} = 0\,,\ t \in [0,T]\,, x \in \Omega\,, \tag{4.1}$$

$$u(x,0) = g(x)\,, \tag{4.2}$$

$$u(x,t) = h(t)\,,\ x \in \Gamma_\Omega\,. \tag{4.3}$$

Here $F(u)$ is the flux function, x belongs to the finite, one-dimensional domain Ω with domain boundary Γ_Ω, and t is the time. We split the domain into N elemental sub-domains Ω^e spanning Ω:

$$\Omega = \bigcup_{e=1}^{N} \Omega^e\,,\ \Omega^e \in [x_a^e, x_b^e]\,.$$

Following the standard Galerkin method, we multiply with a test function $v_h = v_h(x)$, however we integrate over each element individually to get the weak form of eq. (4.1) as

$$\int_{\Omega^e} v_h \frac{\partial u_h^e}{\partial t} \mathrm{d}\Omega + \int_{\Omega^e} v_h \frac{\partial F(u_h^e)}{\partial x} \mathrm{d}\Omega = 0\,, \tag{4.4}$$

where u_h^e represents the discrete version of the solution vector u in Ω^e.

We now specify that $u_h^e, v_h \in \mathscr{U}^p$, where $\mathscr{U}^p$ defines the finite dimensional space of polynomials of degree at most p on Ω^e. Let $\varphi(x) \in \mathscr{U}^p$ be a set of polynomial basis functions. In Ω^e, the solution is approximated as

$$u(x,t) \approx u_h^e(x,t) = \sum_{i=0}^{p} \varphi_i(x) \tilde{u}_i^e(t)\,,\ x \in \Omega^e\,, \tag{4.5}$$

where $\tilde{u}_i^e$ is the coefficient associated with the i^{th} basis function of element e.

Integrating the spatial derivative term in eq. (4.4) by parts, gives

$$\int_{\Omega^e} v_h \frac{\partial u_h^e}{\partial t} \mathrm{d}\Omega + \int_{\Gamma_{\Omega^e}} v_h \hat{F}(u_h^e) \mathrm{d}\Gamma - \int_{\Omega^e} \frac{\partial v_h}{\partial x} F(u_h^e) \mathrm{d}\Omega = 0\,, \tag{4.6}$$

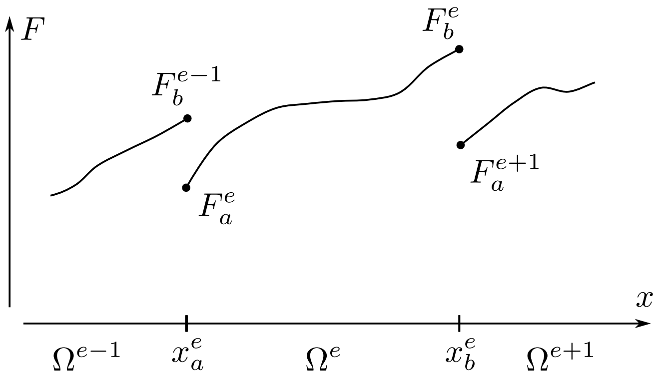

Figure 4.1: The DG discretisation, showing the discontinuous nature of the solution (F in this case). Please note that the domain is continuous, i.e. $x_b^e = x_a^{e+1}$, but the solution is not necessarily so, $F_b^e \neq F_a^{e+1}$.

where the normal boundary flux F has been replaced by a numerical flux approximation $\hat{F}$, which is evaluated at each element boundary.

4.2.1 Nodal or modal basis

The choice of basis function affects the meaning of the coefficient $\tilde{u}_i^e$. In general, we differentiate between nodal and modal bases. A nodal base indicates that each coefficient has a physical meaning, representing the solution at a given point in the element:

$$\tilde{u}_i^e = x_i^* \; \forall i \in [0,1,...,p], \quad x_i^* \in \Omega^e \,. \tag{4.7}$$

In a modal base, there is no such guarantee. To illustrate, a linear interpolation can be achieved by two different sets of shape functions, as in table 4.1. The modal example is here chosen as the two first modes in the Legendre expansion.

Nodal	Modal
$\varphi_0 = 0.5\,(1+\xi)$ $\varphi_1 = 0.5\,(1-\xi)$	$\varphi_0 = 1$ $\varphi_1 = \xi$
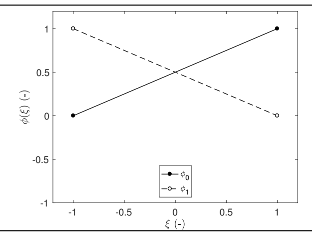	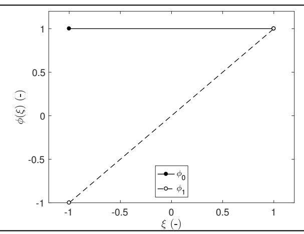

Table 4.1: Illustration of the difference between nodal and modal basis functions for a $p = 1$ solution on the standard domain $\xi \in [-1,1]$.

In the cable model developed in paper V, we have used the modal-type Legendre polynomials as basis functions. Their key feature is their orthogonality

$$\int_{\Omega^e} \varphi_i \varphi_j \mathrm{d}\Omega = \frac{2\Delta^e}{2p+1}\delta_{ij}\,, \tag{4.8}$$

where $\Delta^e = x_b^e - x_a^e$ is the element size. Eq. (4.8) is also the definition of the elemental mass matrix. The orthogonal feature makes the matrix diagonal and hence trivial to invert, which makes the Legendre polynomials a computationally efficient choice of modal basis functions. For more information on different choices of basis functions, see [87].

4.2.2 The numerical flux

In the DG method, the elemental domains are decoupled. The finite element space is piecewise continuous and allows discontinuities at elemental boundaries as depicted in figure 4.1. For a given element edge, shared between element e and $e+1$, we define indices L and R,

$$F_L = F_b^e\,, \qquad\qquad F_R = F_a^{e+1}\,, \tag{4.9}$$

as the left and right solution states respectively. For ease of notation, it is customary to define the trace and the jump operators at the boundary respectively as

$$\{F\} = \frac{1}{2}(F_L + F_R)\,, \qquad\qquad [[F]] = \frac{1}{2}(F_L n_L + F_R n_R)\,, \tag{4.10}$$

where n_L and n_R are the outward pointing normals of the left and right element respectively. In our one-dimensional problem, this is simply $n_L = 1$, $n_R = -1$.

The trick in DG is that the numerical flux $\hat{F}$ in eq. (4.6) is a function of the solution state on both sides of the elemental boundary: $\hat{F} = \hat{F}(u_L, u_R)$. This is the only passage of information between elements in this formulation. The choice of $\hat{F}$ defines the type of solver that emerges from (4.6). In short, the task of the numerical flux is to utilize the finite volume possibility of pure upwinding, or to choose a suitable level of it for the solution. For that we need to know something about the characteristics of the solution, as is well explained in [153]. To illustrate, consider the simple case of a linear advection equation with propagation speed c:

$$\frac{\partial u}{\partial t} - \frac{\partial cu}{\partial x} = 0\,. \tag{4.11}$$

Eq. (4.11) is a pure transport equation where a perturbation in u propagates from left to right in x with speed c. A pure upwind scheme would therefore use $\hat{F} = F_L = -cu_L$ and would be the best choice in this example. Simply taking $\hat{F} = \{F\}$ results in that information downstream of a right-going signal will affect the signal itself (downwinding). In turn, this leads to numerical oscillations and less accurate solutions. An example of a common and simple flux scheme that degenerates to the pure upstream flux for the linear advection case is the Lax-Friedrich (LF) flux (see e.g [37]),

$$\hat{F}^{LF} = \{F\} - |\lambda|_{\max}[[u]] \,, \tag{4.12}$$

where $|\lambda|_{\max}$ is the largest eigenvalue in the system. In eq. (4.11), clearly $|\lambda|_{\max} = c$ and $F(u) = -cu$, which gives

$$\hat{F}^{LF} = 0.5\left(-cu_L - cu_R - (cu_L - cu_R)\right) = -cu_L \,, \tag{4.13}$$

as desired.

The LF flux is very popular due to its simplicity and ease of implementation, but is considered to be quite diffusive for nonlinear advection problems. As the order of the polynomial expansion increases however, the influence of the flux choice decreases and the LF has shown good results in practical computations [37]. For more advanced numerical fluxes, taking different wave types into account, see the book by Toro [153]. The Lax-Friedrich flux is used in Paper V to implement an approximative Riemann solver for cable dynamics.

4.3 The local discontinuous Galerkin Method

Paper I describes a local discontinuous Galerkin (LDG) method for cable dynamics. The LDG method was initially developed for elliptic problems [37]. So, to explain the method we consider the Laplacian problem for u:

$$\frac{\partial^2 u}{\partial x^2} = f \,. \tag{4.14}$$

The LDG method requires the model problem to be written as a first order scheme in space. We therefore introduce an auxiliary variable, q as the spatial derivative of u and express the system of equations as

$$\begin{aligned} q &= \frac{\partial u}{\partial x} \,, \\ f &= \frac{\partial q}{\partial x} \,. \end{aligned} \tag{4.15}$$

Following the steps described in section 4.2, we arrive at the DG formulation

$$\int_{\Omega^e} v_h q_h^e \mathrm{d}\Omega = \int_{\Gamma_{\Omega^e}} v_h \widehat{u}_h^e \mathrm{d}\Gamma - \int_{\Omega^e} \frac{\partial v_h}{\partial x} u_h^e \mathrm{d}\Omega \,, \tag{4.16}$$

$$\int_{\Omega^e} v_h f \mathrm{d}\Omega = \int_{\Gamma_{\Omega^e}} v_h \widehat{q}_h^e \mathrm{d}\Gamma - \int_{\Omega^e} \frac{\partial v_h}{\partial x} q_h^e \mathrm{d}\Omega \,. \tag{4.17}$$

The numerical fluxes of the LDG method are

$$\widehat{u}_h = \{u_h\} + \beta[[u_h]], \tag{4.18}$$

$$\widehat{q}_h = \{q_h\} - \beta[[q_h]] + \eta_1[[u_h]], \tag{4.19}$$

where $\beta \in [-1,1]$ controls from which direction to weight the flux. η_1 is a case-dependent penalty parameter. Please note that in Cockburn and Shu define the jump without the 0.5 factor and consequently, $\beta \in [-0.5, 0.5]$ in the original LDG method. The scheme is named *local* DG because of how the use of q can be eliminated locally by combining the equations above. However, in the case of cable dynamics presented in Paper I, the strong non-linear dependence of q makes this step difficult to realise.

4.4 Shock capturing techniques

The correct handling of shocks (discontinuities) in hyperbolic systems is a widely studied topic, and is e.g. described in detail by Toro [153]. Three important mathematical theorems govern the requirements on numerical schemes for shocks, briefly explained below.

Godunov
: Any linear method which is more than first-order accurate, will in the presence of shocks generate numerical oscillations [73].

Lax-Wendroff
: If a conservative numerical scheme is converging, the solution it converges to will be the correct one [95].

Hoe-LeFloch
: If a non-conservative numerical scheme is converging, the solution it converges to will be the wrong one, if it contains a shock [82].

So, a conservative scheme is needed for correct shock-wave propagation. To avoid overshoots, a monotone scheme must be applied to avoid numerical oscillations (also referred to as Gibbs-type oscillations or over- and undershoots). For finite volume methods, the dominating approach to resolve shocks started with van Leer's limiter scheme, monotone upstream-centered scheme for conservation laws (MUSCL) [160]. The use of a limiter to circumvent Godunov's theorem has spawned a wide range of limiters, applied to the slope or flux of a solution, see e.g. [18] for a list of the most popular methods. The idea of limiting is to keep the second order accuracy of the scheme while avoiding overhoots in the solution, or more precisely ensure that the total variation is non-increasing or bounded (TVD or TVB respectively). Since the limiters are adopted from the finite volume method, they can be readily applied to a DG discretisation, however solutions of $p > 1$ are not supported and the energy content of modes of higher order should be removed if present when the limiter is activated [37].

For high-order methods, Persson and Peraire [131] introduced a sub-cell viscosity to apply a suitable and element local level of viscosity to the solution, thus suppressing the oscillations. The method was introduced in an LDG framework, and was later generalised by Klöckner et al. in [90]. Its main advantage is that it can be applied directly on an arbitrary polynomial order, without having to degenerate to linear elements. The level of viscosity was set for each element by the use of a smoothness indicator. They used the difference between the solutions of order p and $p-1$ to approximate the smoothness of the solution.

The paper by Krivodonova [91] introduced another notion for shock detection. She proposed to use the expected order of convergence of the elemental jumps to approximate the discretisation error and separate smooth regions from regions with sharp gradients. This is the approach that is implemented in Paper V.

4.5 Adaptivity

The DG framework is very well suited for problems with non-smooth regions, either in the geometry of the problem or in the solution itself [37]. The elemental nodes can be non-conforming, i.e. element neighbours can have different size and polynomial order, because all element inter-connectivity is managed by the numerical flux. This makes adaptive mesh refinement more easy to implement. Mesh adaptivity is also suitable for the limiter approach of shock-capturing schemes. By using an error indicator compared with a given tolerance level, the mesh can be refined in regions where the discretisation error is high. The error indicator can be based on either the inter-elemental jumps as in e.g. [19], or the approximation difference in polynomial order as in e.g. [52].

An element in a DG mesh can adapt to the solution by changing its polynomial order ($p-$adaptivity), change the elemental size by deforming ($r-$adaptivity), change the elemental size by splitting into more elements or merging with neighbouring ones ($h-$adaptivity), or any combination of the three. In Paper V we develop an $hp-$adaptive mesh refinement scheme. As such, we allow for elemental splitting/merging operations and account for that any element can carry solutions of any polynomial order.

The aim of an $hp-$adaptive scheme is to utilize the convergence rate $\varepsilon = \mathscr{O}\left(h^{p+1}\right)$ for smooth solutions in an efficient manner, while maintaining good accuracy around discontinuities [153]. Therefore we must separate smoothness indication from error indication. In smooth regions with a high error, we should increase p to achieve an efficient convergence. But if a shock is present, higher p will only increase the overshoot and the non-physical oscillations, and we should go to linear elements and limit the solution using a slope limiter. The performance of an $hp-$adaptive scheme is very much dependent on reliable and robust indicators for both the discretisation error and the smoothness of the solution. Paper V describes an $hp-$adaptive control algorithm used for cable dynamics.

5

Summary of work

5.1 SOFTWARE DEVELOPMENT

This thesis presents the development of Moody, an *hp*-adaptive finite element model of mooring cables. Three major versions of the software have been developed during the project. Their main features and the papers in which they have been used are presented in table 5.1.

Table 5.1: Overview of features in the three main Moody versions, labelled by release year. The API (Automated Program Interface) column refers to the interpolation order used to sub-step the boundary conditions in coupled mode. LDG stands for the local discontinuous Galerkin method formulation, and LF denotes a local Lax-Friedrich Riemann solver.

Version	Papers	Language	Formulation	API	Adaptivity
v2013	I, II	Matlab	LDG	linear	no
v2015	IV	C++	LDG	quadratic	no
v2017	V	C++	Riemann (LF)	quadratic	yes

The main driving force for re-implementing the LDG method in C++ was computational speed. A speed-up factor in the order of 20-50 was achieved by simply changing the program language. A C++ implementation also made coupling to high performance computing clusters more robust, compared to the previously used Matlab coupling, that we developed in [113].

Moody was from the start intended to be a mooring module to different solvers for the hydrodynamic problem, i.e. for coupled analysis of moored objects. This required setting up an Automated Program Interface (API) to communicate between software.

API

The design of the API is centred at the question of multiple time scales. Early versions of the API simply used the first-stab approach of linearly interpolating the position of the mooring point between coupling times. A linear interpolation of the Dirichlet boundary conditions of position, $r_{\mathrm{D}}(t)$ and velocity, $v_{\mathrm{D}}(t)$, over a time step size $\Delta t = t_{k+1} - t_k$, is expressed as

$$r_{\mathrm{D}}(t) = \frac{r_k\,(t_{k+1} - t) + r_{k+1}\,(t - t_k)}{\Delta t}\,, \tag{5.1}$$

$$v_{\mathrm{D}}(t) = \frac{r_{k+1} - r_k}{\Delta t}\,, \tag{5.2}$$

where r_k is the position of the mooring point at time t_k. See also figure 5.1. This worked decently in the coupling to OpenFOAM as the time step restriction of the CFD solver itself was sufficiently low. However, to use Moody with larger coupling time steps (e.g. for coupling with faster hydrodynamic models), designing a better interpolation was important.

The difficulty lies in the causality of the coupling problem. At a given coupling time, we do not know the next point, making a smooth transition difficult to accomplish. For signals with high acceleration per sample step, the discontinuous velocity shown in figure 5.1(b) induces substantial numerical noise in the cable formulation. A staggered quadratic interpolation scheme was therefore developed for Paper IV.

To explain, we let t_k and t_{k+1} be two consecutive coupling times, with corresponding mooring point positions r_k and r_{k+1}. We introduce the lag-time fraction $\phi \in [0,1]$ and identify a corresponding mooring time $t^{\mathrm{m}}_{k+1} \in [t_k, t_{k+1}]$ as

$$t^{\mathrm{m}}_{k+1} = \phi t_k + (1-\phi)\,t_{k+1}\,. \tag{5.3}$$

The mooring boundary conditions $r_{\mathrm{D}}(t)$ and $v_{\mathrm{D}}(t)$ are interpolated over the mooring time step interval $t \in \left[t^{\mathrm{m}}_k, t^{\mathrm{m}}_{k+1}\right]$ as

$$r_{\mathrm{D}}\left(t^{\mathrm{m}}_k + \tau\right) = r^{\mathrm{m}}_k + v^{\mathrm{m}}_k \tau + 0.5 a_k \tau^2\,, \tag{5.4}$$

$$v_{\mathrm{D}}\left(t^{\mathrm{m}}_k + \tau\right) = v^{\mathrm{m}}_k + a_k \tau\,, \tag{5.5}$$

where $\tau \in \left[0, t^{\mathrm{m}}_{k+1} - t^{\mathrm{m}}_k\right]$, while $r^{\mathrm{m}}_k = r_{\mathrm{D}}\left(t^{\mathrm{m}}_k\right)$ and $v^{\mathrm{m}}_k = v_{\mathrm{D}}\left(t^{\mathrm{m}}_k\right)$ are taken from the previous coupling interval. To close the system, we only need to define a_k. Here, we choose a_k as the constant acceleration needed to satisfy $r_{\mathrm{D}}\left(t_{k+1}\right) = r_{k+1}$, i.e.

$$a_k = \frac{r_{k+1} - r^{\mathrm{m}}_k - v^{\mathrm{m}}_k \Delta_k}{0.5\Delta_k^2}\,, \tag{5.6}$$

with $\Delta_k = t_{k+1} - t^{\mathrm{m}}_k$.

Figure 5.1 shows an example of the effects of using different interpolations. Resulting interpolation using a coupling interval of $\Delta t = 0.05\,\mathrm{s}$ with 50 sub-steps

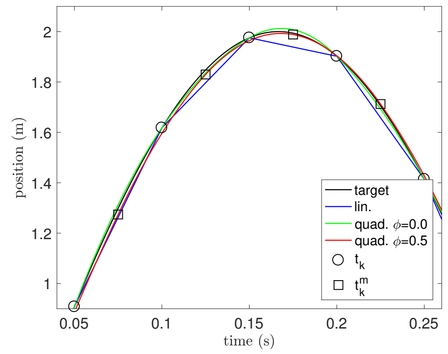

(a) Position

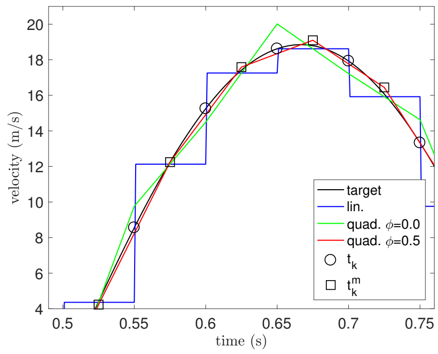

(b) Velocity

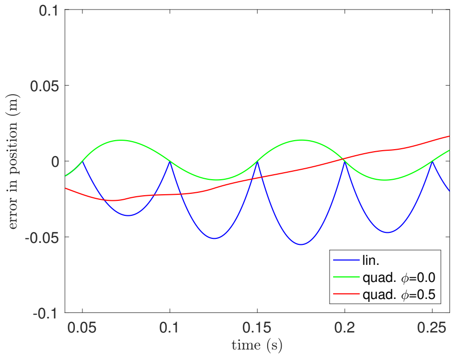

(c) Position error

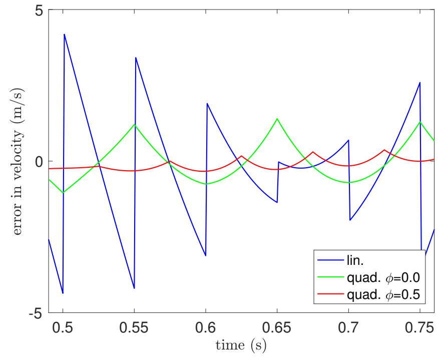

(d) Velocity error

Figure 5.1: Effect of different approaches to interpolation of Dirichlet boundary conditions in coupled simulations. Results for linear interpolation (lin.), and quadratic interpolation (quad.) of position are shown. ϕ denotes the lagging fraction of the quadratic interpolation. Interpolated results of (a) position, and (b) velocity are shown, with corresponding error difference to the target shown in (c) and (d). Please note that (a) and (b) are examples to show the interpolation quality, and are therefore chosen from different time intervals of the sinusoidal position signal.

is shown. It shows part of a coarsely sampled sinusoidal signal, for linear interpolation, quadratic interpolation and staggered quadratic interpolation of half a time step, $\phi = 0.5$, respectively. The target signal in figure 5.1(a) is best matched by the $\phi = 0$ quadratic interpolation as it always has the exact solution at the coupling times. The lagging counterpart has slightly larger deviations from the signal. However, we note that the smoothness of velocity in the staggered version is very much improved. The smoothness of both signals is important for the quality of the mooring simulation. In terms of accuracy in the coupling, we argue that returning a staggered force amplitude is a small prize to pay for a good resolution of both boundary condition signals needed for the simulation. This sample resolution is of course too low to provide a high-quality coupled simulation. In practical appli-

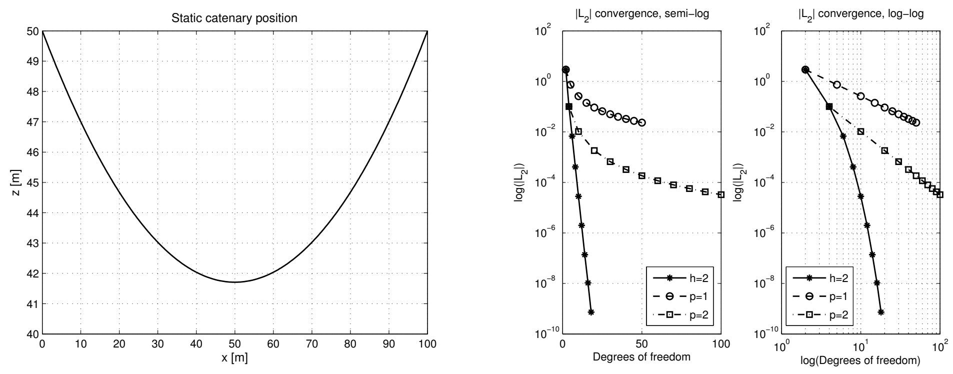

(a) Static configuration (b) Position convergence

Figure 5.2: Paper I: Static convergence of the LDG discretisation. (a) shows the catenary shape studied. (b) the convergence of position in the L_2 norm with increasing polynomial degree on two elements (h=2) and with increasing number of elements on a $p = 1$, and $p = 2$ order meshes.

cations a better temporal resolution is used, resulting in decreasing errors caused by using the staggered scheme.

5.2 A LOCAL DISCONTINUOUS GALERKIN FORMULATION - PAPER I

A numerical model for mooring cable dynamics based on the local discontinuous Galerkin (LDG) method of Cockburn and Shu [35] is presented in Paper I. The LDG method requires a first order system in space, as described in chapter 4. In the context of cable dynamics, we therefore introduce the auxiliary variable $q = \partial\vec{r}/\partial s$. The LDG scheme fluxes are implemented according to [37], with an extra penalty term η_2 penalising the velocity jump. See Paper I for more information on the details of the formulation.

Simulations of a static hanging catenary shows the expected exponential convergence of smooth solutions, see figure 5.2.

Figure 5.3 shows the unfiltered results from simulations with 10 elements of order 7 compared with experimental data for a single catenary chain subjected to harmonic, circular fair-lead motion. There is an excellent agreement between the tension force time histories from the numerical model and the measured values. In the low-tension regime we note numerical noise, which is a consequence of neglecting the bending stiffness of the cable, in combination with the numerical difficulty of a discontinuous contact force from the ground in the touch-down region of the cable. However, the dynamic behaviour around the tension crests matches the experimental data well.

One major disadvantage of the LDG formulation is that the tension force $T(\vec{q})$ becomes a function of a fluxed variable ($\vec{q}$). This means that the tension force can-

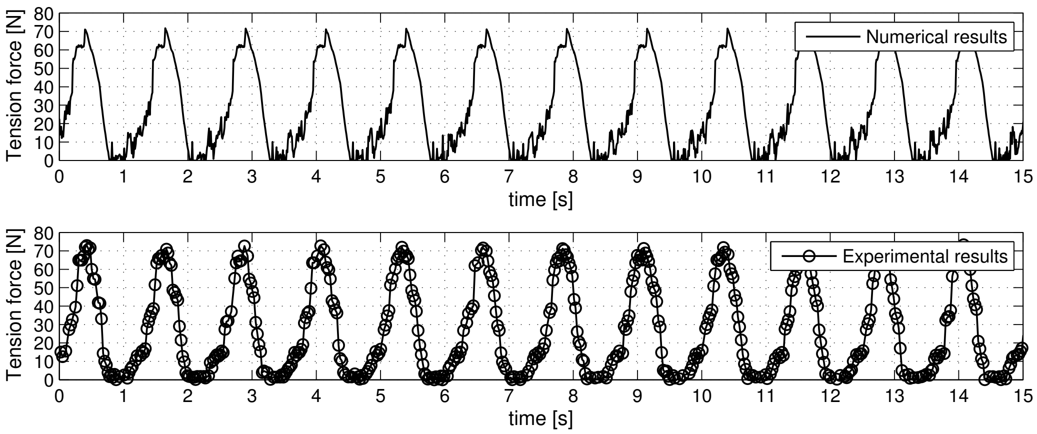

Figure 5.3: Paper I: Comparison of fair-lead tension with experimental data. Results are from a forced circular end-point motion with a radius of 0.2 m, with a 1.25 s period time.

not be post-processed locally from the elemental solution, but need boundary conditions for accurate reconstruction. It was also difficult to find a case-independent choice of penalty terms (η_1 and η_2), and the application of limiters was problematic. These drawbacks were the main motivators for the development of the Riemann solver used in Paper V. Nevertheless, we conclude that the Paper I model gives reliable results for catenary mooring systems and that the modified LDG method is stable for cable dynamics, including cases with cable slack and snap loads.

5.3 Coupled CFD-mooring analysis - Paper II

CFD simulations of a moored generic point-absorbing WEC were made using finite volume VOF-RANS simulations as implemented in the OpenFOAM platform [110] (OF). Fifth order regular Stokes waves were used to simulate the motion of the device with and without mooring cables and power take off (PTO). The native rigid body solver in OF was modified to include mooring forces from nested Moody simulations, and a simple API was developed to couple the solvers (OF and Moody). The results were produced using the v2013 version of Moody, with linearly interpolated boundary conditions.

Figure 5.4 shows the heave response per wave height in regular waves with 5 s period time for the four combinations studied (free or moored, and with or without PTO). We notice a clear wave height dependence on the response amplitude operator (RAO), i.e. the ratio between response amplitude and wave amplitude. The RAO decreases as the wave height increases. In retrospect, the results were in agreement with the findings of Yu and Li [177]. At the time however, the results were considered indicative because the simulations had an under-resolved boundary layer, which most likely over-estimated the viscous damping on the body mo-

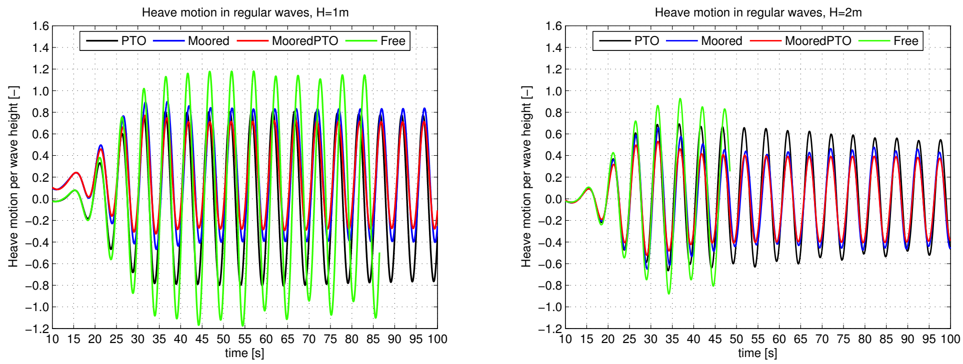

(a) $H = 1$ m (b) $H = 2$ m

Figure 5.4: Paper II: Heave results of four simulation settings: free floating buoy; only PTO; only moored; and moored with PTO. The motion response is divided by incoming wave height, H. $H = 1$ m in (a) and $H = 2$ m in (b).

tion. The Laplacian solver for mesh motion (in version 2.1.x of OF) had problems with skewed cells close to the corners of the buoy for large pitch motions. This caused the simulation to crash, as can be seen from the premature ending of the free response curve in figure 5.4. Increasing the boundary layer resolution, resulted in illegal cells at even smaller degrees of pitch response. Hence we chose to focus on the coupling and to show that the method worked. For further analysis of the results, a validation study was needed.

Figure 5.5 shows a simulation of the body in an extreme wave, where we see a mooring design failure (vertical loads on a drag-embedded anchor) in figure 5.5(a). Of special interest is the force time history in figure 5.5(b). A snap load is generated in the low tension region and is repeatedly reflected and propagated in the cable. This example shows the importance of snap load accuracy. Both amplitude, propagation and damping rate of the tension force will affect the load cycle history, and thus the expected life-time of the mooring cable.

Paper II shows the possibility to use coupled CFD-mooring analysis to compute the moored motion of floating WECs. The model complexity is very high, as is the required computational effort, but it has very few underlying assumptions and few parametrised variables. Many of the non-linearities expected to influence the WEC response are inherent in the model, including non-linear and breaking wave kinematics, viscous forces, over-topping, instantaneous wetted surface, dynamic mooring response, and PTO forces.

5.4 Experimental work - Paper III

A generic cylindrical buoy with three different mooring configurations was modelled in a physical experiment. The buoy was moored with three symmetrically

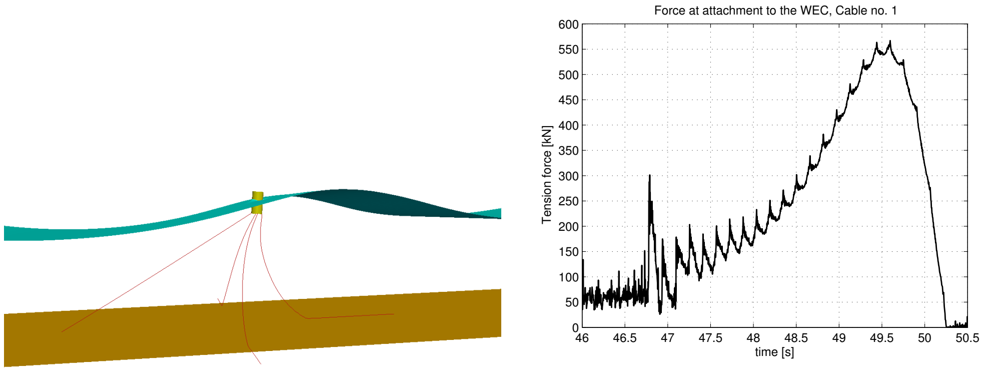

(a) (b)

Figure 5.5: Paper II: Results from a $H = 15$ m wave height, $T = 12$ s period time wave. In (a) we see a mooring failure, as the full seaward line is lifted. (b) shows the tension time history of the fair-lead of the seaward cable.

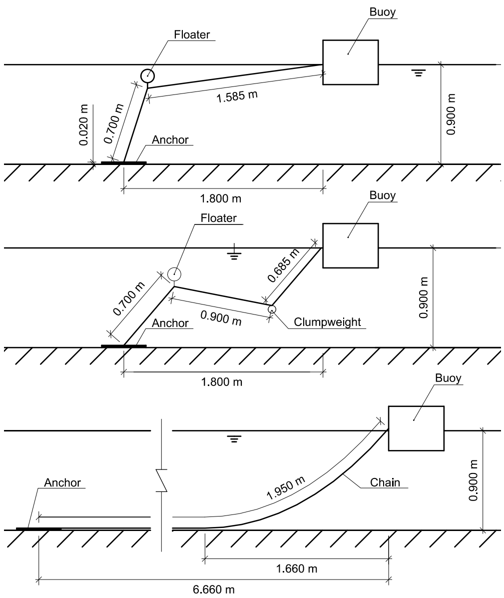

Figure 5.6: Paper III: Side view of the different mooring configurations. From top to bottom: CON1, CON2, CAT.

placed mooring legs. The mooring leg configurations studied were comprised of:

CON1 a synthetic cable with an intermediate floater;

CON2 a synthetic cable with an intermediate sinker and a floater;

CAT a catenary chain.

Figure 5.6 shows the profiles of the mooring legs in the three configurations.

Table 5.2: Paper III: Results from operational sea-state tests. τ_1 - tension in seaward cables; τ_2 - tension in leeward cable; η_1 - surge; η_3 - heave; p.p - peak-to-peak amplitude. Overbar denotes mean value.

	OP1			OP2		
Parameter	CON1	CON2	CAT	CON1	CON2	CAT
H_s (m)	0.031	0.031	0.029	0.034	0.033	0.033
T_P (s)	0.90	0.90	0.90	1.28	1.28	1.30
$\max \eta_1$ $(\cdot 10^{-3}\,\mathrm{m})$	46.2	43.8	43.3	47.4	43.6	40.0
$\overline{\eta}_{3p.p}$ $(\cdot 10^{-3}\,\mathrm{m})$	9.1	8.5	8.5	25.3	25.1	24.5
$\overline{\dot{\eta}^2}_3$ (m^2/s^2)	0.048	0.039	0.040	0.271	0.263	0.250
$\overline{\tau}_1$ ($\pm 0.2\,$N)	2.9	10.8	3.1	2.9	10.7	3.1
$\max \tau_1$ ($\pm 0.2\,$N)	5.8	11.9	3.6	5.1	12.1	3.9
$\min \tau_1$ ($\pm 0.2\,$N)	0.2	9.6	2.7	0.7	9.2	2.4
τ_{Dyn1} ($\pm 0.3\,$N)	2.9	1.1	0.5	2.2	1.5	0.8
$\overline{\tau}_2$ ($\pm 0.2\,$N)	3.0	11.1	3.0	3.0	11.1	3.0
$\max \tau_2$ ($\pm 0.2\,$N)	6.6	12.3	3.6	5.9	12.6	3.8
$\min \tau_2$ ($\pm 0.2\,$N)	0.1	9.9	2.5	0.3	9.3	2.0
τ_{Dyn2} ($\pm 0.3\,$N)	3.6	1.2	0.6	2.9	1.6	0.8

Mooring system compliance and stiffness are important parameters for the dynamic response. Therefore the mooring configurations were designed to have the same hydrostatic stiffness (at the equilibrium position) in the surge direction. This enabled a more direct comparison between the results from different configurations because we expected similar behaviour in static offset due to drift forces. Indeed, the configurations proved to behave similarly over a range of frequencies of regular waves.

In operational conditions, the peak to peak value of the motion response, in combination with the dynamic range of the mooring forces are the most important factors to measure the mooring performance. Table 5.2 shows parts of the results from the operational sea-states, where we focus on the maximum drift offset, the heave response and the mooring loads. In terms of heave response, there are some differences between the configurations. Overall CON1 had a slightly better performance than CON2, which in turn outperformed CAT. But, the relative performance is reversed in terms of mooring force response where the catenary has the smallest dynamic range in all three mooring legs.

In survival sea-states, the performance criteria change in favour of station-keeping and mooring force response. The best performing mooring is the one which limit the buoy response enough, while still keeping the mooring forces to a minimum. Table 5.3 shows parts of the results from the survival sea-states,

Table 5.3: Paper III: Results from survival sea-state tests. τ_1 - tension in seaward cables; τ_2 - tension in leeward cable; η_1 - surge; p.p - peak-to-peak amplitude. Overbar denotes mean value.

	SURV1			SURV2		
Parameter	CON1	CON2	CAT	CON1	CON2	CAT
H_s (m)	0.083	0.084	0.082	0.094	0.096	0.093
T_P (s)	1.16	1.16	1.16	1.39	1.39	1.39
$\max \eta_1$ ($\cdot 10^{-3}$ m)	311.6	318.6	278.7	186.8	222.7	210.8
$\overline{\tau}_1$ (± 0.2 N)	3.6	11.2	3.8	3.2	11.0	3.4
$\max \tau_1$ (± 0.2 N)	11.0	17.3	17.5	9.6	14.8	11.2
$\min \tau_1$ (± 0.2 N)	0.0	6.5	0.2	0.0	7.8	0.3
τ_{Dyn1} (± 0.3 N)	7.4	6.2	13.7	6.4	3.9	7.8
$\overline{\tau}_2$ (± 0.2 N)	2.3	10.5	2.4	2.6	10.7	2.6
$\max \tau_2$ (± 0.2 N)	8.9	15.1	8.6	8.0	13.6	6.6
$\min \tau_2$ (± 0.2 N)	0.0	5.7	0.5	0.0	7.1	0.7
τ_{Dyn2} (± 0.3 N)	6.5	4.6	6.2	5.4	2.8	4.0

focusing on mooring loads and the maximum surge offset. We highlight that the minimum tension of CON1 is 0.0 in both sea-states and in all mooring legs (seaward and leeward), which would make it prone to snap loading. Here, the dynamic tension is the smallest in CON2, while CAT shows the highest values, indicating that we indeed get large load amplification when moorings go slack.

Results from modelling regular waves, operational sea-states and survival sea-states highlight the complexity of choosing an optimal mooring design. A suitable mooring layout will have to be found by careful consideration of all aspects of the site conditions and of device specific demands on the mooring.

5.5 Validation of the coupled model - Paper IV

A CFD model of the physical experiments in Paper III was set up to validate the coupled VOF-RANS model. The catenary configuration was modelled in Moody, and the coupled response was studied using the improved API with quadratic interpolation of the fair-lead position in time (v2015). Results from decay tests in surge, heave and pitch were compared, with excellent agreement in surge and heave. We highlight the matching surge response in figure 5.7. The surge motion is dominated by the mooring response, and as such, the good agreement gives confidence that the coupled model gives reliable results.

Simulation results in regular waves of three different periods, at two different wave heights show a very good agreement with the experiments, except in pitch

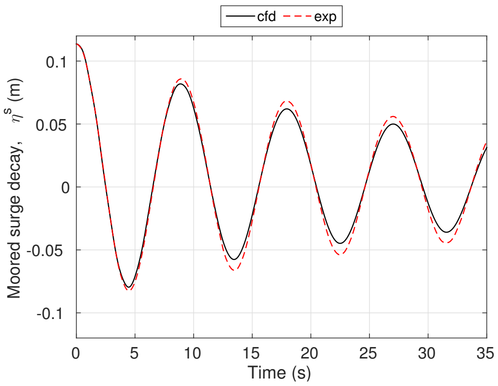

Figure 5.7: Paper IV: Time history of surge decay, comparison between experimental data and numerical results.

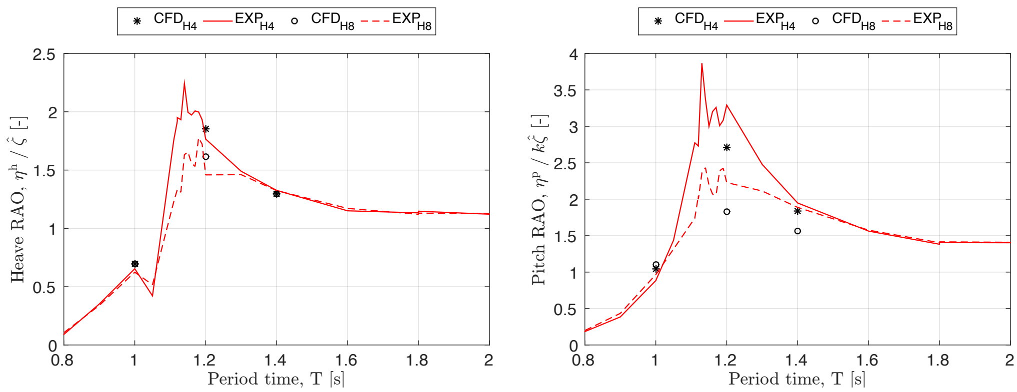

(a) Heave

(b) Pitch

Figure 5.8: PaperIV: Response amplitude operators for heave and pitch from experiments, compared with CFD results.

where the model was very sensitive to input parameters. Due to small geometric uncertainties and simplifications, the numerical model overestimated the pitch damping and the natural frequency of the pitch response compared with the experimental results. This contributed to the under-estimated pitch response in figure 5.8.

The most important result from this study is that the numerical model provides a good estimation of the non-linear RAO seen in the experimental results. This is done with very few parametrised forces and thus provides a good platform for further quantification of the underlying hydrodynamic factors causing this behaviour.

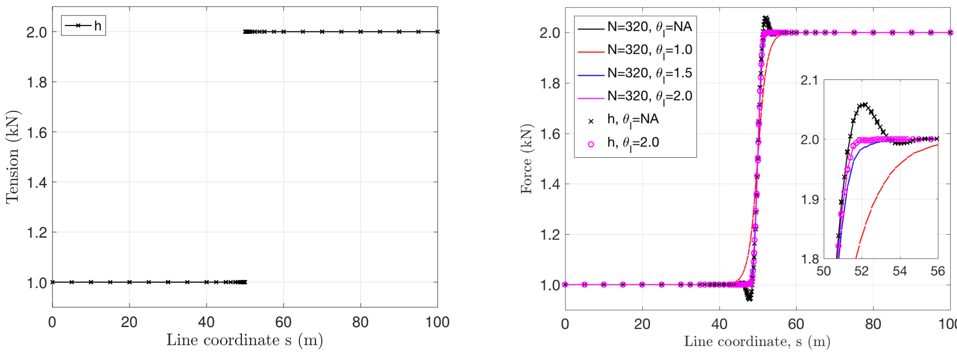

(a) t = 0 s (b) t = 2 s

Figure 5.9: Shock front appearance. (a): Initial condition of tension, also showing the h-adapted mesh in 5 levels with markers on quadrature points. (b) Shock front after 1 return period for different values θ_l on 320 static elements, and the 5-level $h-$adapted solution.

5.6 Capturing snap loads - Paper V

Now we return to the modelling of cable dynamics. For the purpose of capturing snap loads, we rewrite the cable equation of motion in conservative form:

$$\dot{u} = \frac{\partial F(u)}{\partial s} + Q(u)\,. \tag{5.7}$$

The solution vector is here $u = [r,\, q,\, v]^{\mathrm{T}}$, where $v = \dot{r}\gamma_0$ (kg/s) is the cable momentum density. An eigenvalue analysis of the system proves the hyperbolic nature of the problem and pin-points the longitudinal and transverse wave celerities as

$$c_t = \sqrt{\frac{\partial T}{\partial \varepsilon}\gamma_0^{-1}}\,, \qquad\qquad c_n = \sqrt{\frac{T}{|q|\gamma_0}}\,,$$

respectively. The equations are solved using a DG method based on the local Lax-Friedrich approximative Riemann solver as described in [37].

An adaptive control algorithm is implemented to allow $hp-$adaptivity of the cable discretisation. It is based on the jump-based error estimator used in [19] together with the smoothness indicator of [91]. It is also extended to incorporate a criteria for cable slack. The tension force magnitude T is chosen as a control variable for the adaptive scheme.

Figure 5.9 shows the result of a one-dimensional benchmark test of the adaptive algorithm. An initial strain discontinuity is propagated along a linear-elastic cable, and the adaptivity refines the mesh surrounding the tension jump. To avoid excessive overshoots and undershoots close to solution discontinuities, we apply the generalised minMod limiter of [37] to the solution, see $\theta_l = 2$ in fig. 5.9(b). Results from more diffusive limiters with $\theta_l = 1.5$ and $\theta_l = 1$ are also shown for

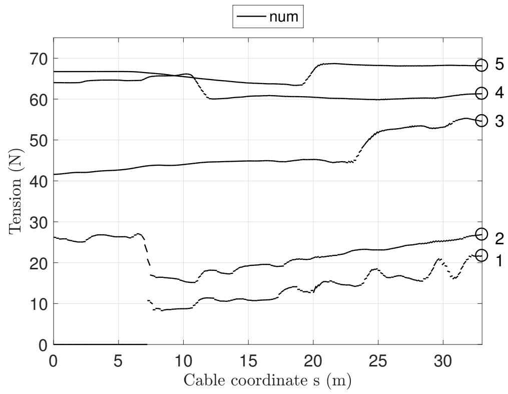

(a) Cable tension snap-shots

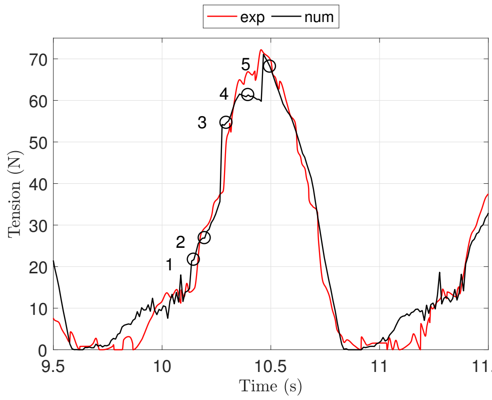

(b) Fair-lead tension

Figure 5.10: Explanation of the dynamic properties of the fair-lead tension time history. (a) shows 5 snap shots of the cable tension along the cable length. Graph no. 1 shows the formation of the shock at $t = 10.10$ s, and numbers 2-5 show the tension force evolution between $t = 10.15$ s and $t = 10.45$ s, sampled every 0.1 s. (b) compares the simulated fair-lead tension history with experimental data. The times of the snap shots in (a) are marked by black circles.

comparison. The results from simulations with a constant mesh of $N = 320$ elements and with a five level $h-$adaptive mesh, starting at $N = 10$ elements and ending at $N = 43$ elements in the limited case, are found to be equivalent. In this idealised case, the adaptive scheme is much more efficient than the static mesh for the same level of accuracy.

The model was also tested using a nonlinear cable material by implementing an exponential strain-force relation. Inspired by the tests and analytical work presented by Tjavaras [152], results from shock propagation tests show good estimates of both force reflection coefficient and nonlinear shock speed.

We revisit the experimental test from Paper I for validation of the new formulation. For a $N = 10$ element base mesh with four layers of h-refinement, the results are very well matched with the experimental data, see figure 5.10. This detailed study of the fair-lead tension history shows the tension along the cable at five time instants during the upstroke of the motion. We can clearly see the relation between the snap load propagation and the appearance of the tension force time history.

5.7 Further mooring studies

Admittedly the experiments from Lindahl [99] were used for validation in both Paper I and Paper V, and preferably more tests should have been used. However, Moody has been compared with experimental data in several other publications (not appended). First, we note that the full test-suite of [99] was used as an ex-

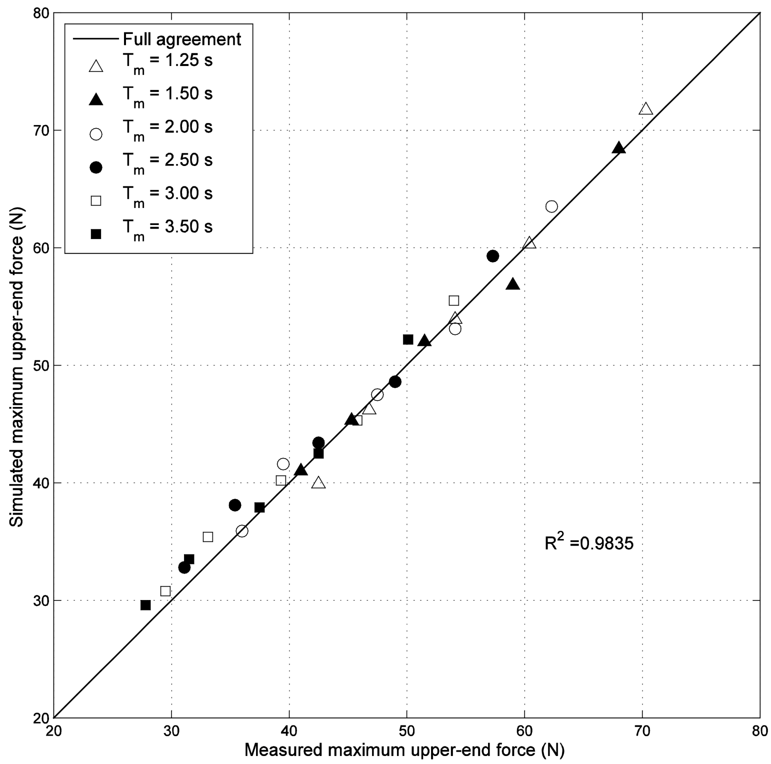

Figure 5.11: Simulated, versus maximum upper end force for various excitation periods T_m (s) and radii r_m (m). From Bergdahl et al. [17].

ample validation in [17]. The results are shown in figure 5.11 and show excellent agreement in maximum tension force over a range of circular end-point motion tests for different radius-frequency combinations.

Forced end point motion simulations were used to compare with experimental data in [59]. We showed good results, but also showed how mooring results in small scale are highly sensitive to measurement noise in the motion history. Comparison with experimental data was also presented in [161], including a comparison with the Orcaflex software [111] with some differences noted. In [174], Yang et al. compared Moody results with the DEEPC mooring solver [48] showing similar mooring response but large differrences in fatigue estimation due to the high-frequency content of the tension history in Moody. In coupled mode, the dynamic behaviour has compared well with earlier experiments from Porto: through a linear radiation-diffraction approach in [124] and through coupled CFD analysis in [119]. Finally, we can also mention the validation study on the coupled model from Paper IV. All in all Moody has been used in several test cases of different scales showing reliable results.

6 Discussion

This chapter highlights the key results and elaborates on some of the main challenges in numerical modelling of moored wave energy converters (WECs). We begin with the numerical modelling of mooring dynamics.

6.1 Modelling mooring dynamics

Both the static convergence in figure 5.2 and the dynamic convergence in papers I and V show how well high-order finite elements approximate smooth solutions. The algebraic convergence of increasing the number of elements is not as efficient in reducing the error as is increasing the polynomial order of the element. The order of convergence is theoretically $\mathscr{O}\left(h^{p+1}\right)$ [87], however in Paper V we present convergence results comparing better to a sub-optimal convergence order of $\mathscr{O}\left(h^{p+1/2}\right)$. This is shown for both position r and velocity v. At present, we have no explanation for this sub-optimal convergence.

Table 5.1 shows that there have been three major versions of the code. Most of the external cooperation studies referred to in section 5.7 were made with the earliest version. If we compare Paper I and Paper V, we see that the basics of the formulations are very similar, and for smooth cases we expect small differences between the versions. In terms of the high-frequency tension response however, the snap-load capturing capabilities of the Paper V version is where we expect a better differentiation of numerical noise and physical high-frequency content in the tension force. Paper V further shows that the conservative form of the Lax-Friedrich solver shows correct shock speed and correct reflection on fixed boundaries also in the case of non-linear material response.

Figure 5.10 shows the influence of the formation and reflection of a snap load on the tension force time history from the experiments in [99]. Although well matched in general there are some discrepancies between the experimental data and the numerical results. These are primarily connected to the modelling of external force discontinuities and the treatment of cable slack-snap conditions.

External force discontinuity

There are two points of discontinuity in the external force of the validation case. One is when the cable passes through the free surface, where the fluid density changes rapidly. The density is sampled at each quadrature point and then used to compute the buoyancy and the Morison forces (see section 3.2). This is a relatively weak non-linearity, but one that affects the noise level in the low tension regions. The other, and much more influencial point of interest is the touch-down point where the cable hits the ground. The ground is modelled using a bi-linear spring-damper similar to that of Orcaflex [111] and that used by Gobat [71] who used it to compute snap loads arising at the contact point. The latter concludes that this ground model is suitable for the touch-down region of chains, based on results from an implicit time stepping scheme. However, in our explicit scheme the point of contact is a discontinuity that generates some noise that the limiter is unable to suppress.

An intuitive remedy for the numerical oscillations would be to smear the discontinuity over a given distance, say δ. This could potentially smear the force using a smooth hyperbolic tangent crossing, but the value of δ will now start to affect the solution. Some tests along these lines have been made without achieving robust improvement. To keep the number of tuning parameters to a minimum, this route of development has not been used in computing the results.

The limiter used in the results of Paper V is the generalised minMod limiter described in [37], which is a simple and effective limiter. Possibly, the results could be improved by more advanced choices, but we have not investigated how the use of other limiters might influence the results, beyond what is shown in figure 5.9.

The numerical peak tension in figure 5.10 matches the experiments very well, but it is due to a combination of a slight under-prediction of the smooth peak, combined with an over-predicted snap load. The instantaneous appearance of the tension along the cable shows that the initial snap has very little overshoot. In that respect, the numerical scheme for limiting the sharp gradients works well. The key remaining factor is then the damping of the tension shock. The results in figure 5.9(b) show that the numerical scheme supports shock propagation in the cable with little numerical diffusion. The drag damping effect is very small in the tangential direction, and therefore the dominating damping comes from ground friction. The tangential contact force is modelled using a simple dynamic friction model based on the static normal force of the cable. There were no measurements of the frictional losses in the cable during the experiments, so there is an uncertainty in the friction coefficient and the friction model used. We also note that no internal damping of the chain was modelled. The inclusion of material models with a strain history dependence will be important for more accurate control of the shock dissipation. This is part of an ongoing research project funded by the

Swedish Energy Agency.

The treatment of the ground is more complicated in actual mooring design calculations. Depending on the type of soil and bathymetry at an installation site, the dynamic response changes and the importance of touch-down generation of snap loads becomes difficult to assess numerically. It is costly to do three-dimensional scans, to take soil samples or to do geological surveys of the bottom at the installation site. If the mooring chains are expected to interact with the ground, it is advised to do a wide range of sensitivity studies on how the ground model parameters affect the resulting cable response in the touch-down region.

Slack-snap conditions

We notice some numerical noise in the low-tension region of figure 5.10. The numerical formulation is stable under zero tension, but its accuracy is questionable. Although neglecting bending stiffness is perfectly accurate for a chain, the neglected rotational inertia and the lack of bending friction in the numerical model start have influence in the low tension region. When the tension dissapears, the system looses all stiffness and degenerates to a free-fall condition for the cable. The terminal velocity of the submerged cable is dominated by the drag force acting on the cable [147], making the normal drag coefficient an important parameter. This coefficient was also found to be the most influencial in the sensitivity analysis made in [99]. As described in Paper V, the zero-tension criterion is used as an additional detection of shocks in the solution. This serves two purposes: one is that we ensure a high-resolution treatment of the low-tension region; another is that the ensuing snap load can be readily resolved.

Modern moorings are moving away from catenary chains with drag-embedded anchors [60]. For wires and ropes at low tension, the bending action becomes an important parameter for the ensuing snap load formation, see ch. 38 in [47]. Including bending stiffness is still ongoing work, but a formulation similar to that of Raknes et al. [132] would enable the bending action to be modelled in a global coordinate system with only little modification to the formulation of Paper V. This is the main development path needed for Moody to cover a wider range of mooring applications with better accuracy. All indications point to that it will also decrease the numerical noise in the low tension region of the cables.

Design implications

The ultimate aim of the adaptive scheme presented in Paper V is to increase the computational efficiency and decrease the need of mesh refinement studies in mooring design. A suitable mesh is often chosen based on results from a subset of reference load cases. In moorings that undergo large displacements and possibly large deformation, the response is highly non-linear and it is difficult to know beforehand which cases that are most suitable. This leaves either an uncertainty in the method, or a full test matrix where each load case is tested with a range of meshes. Instead, if a tolerated discretisation error can be used as an input to the $hp-$adapting scheme, there is a large potential in increasing the accuracy as well as the efficiency of the mooring design calculations. This is of particular importance for automated parameter sweeps where only certain output variables are analysed for each case.

6.2 Experimental data for validation

We highlight the conclusion in Bergdahl et al. [17], that the experiments from Lindahl [99] are suitable for validating numerical solvers of cable dynamics. The scale of the experiments (33 m long cable, 3 m water depth and 30-70 N maximum force) makes them rather insensitive to measurement inaccuracies of both material parameters and end-point motion used to generate boundary conditions. If we compare with the data in Paper III, the peak tension of the catenary mooring in a survival seastate was 17.1 N, with a mean tension of 3.8N. Clearly this has a large impact on the accuracy of the measurements needed for a good validation. Small scale model tests are common and suitable for investigation of hydrodynamic parameters, but mooring force signals are more affected by noise in the input data, as is also discussed in [59].

In their review of nonlinear models of WECs, Wolgamot and Fitzgerald [172] conclude:

> ”Many of the experimental comparisons made at this early stage are compromised, to some degree, by the fact that the objective of the experiments is something other than providing good data for CFD validation.”

Paper III and IV combined were designed with the partial aim to achieve just that: ”good data for CFD validation”. It is surprisingly difficult to design experimental test suites with a dual purpose of providing physical understanding of a range of design conditions, while putting enough effort into making the tests simple enough for useful validation. We encountered several problems during the experimental campaign: (i) material manufacturing limitations created a buoy with bulged corners as opposed to a truncated cylinder; (ii) the sensitivity of the load cells for mooring measurements was limited when compared to the accuracy needed by high-fidelity models; and (iii) acceptable measurement uncertainty can have visible effects on the results of a numerical simulation, as was shown in Paper IV in the case of pitch decay.

The model experiments presented in Paper III were made at a scale of 1/100 to full scale. Uncertainties in mooring readings, the accuracy of the rigid body motion capture system and the values of material parameters are all affected by the small scale. We argue that there is still a need for large-scale model tests with a focus on mooring dynamic response and coupled motion during large amplitude motion of a WEC, preferably with and without a power take off system.

However, Paper III should not only be evaluated as a source of validation data. Its main objective was to compare performance of three plausible mooring configurations in different sea-states. Although similar response operators were achieved, with only some differences noted, the response in full sea-states were very different. The mooring load response is strongly influenced by slack-snap events when they occur, and it is clear that the catenary mooring is the most exposed to this type of events.

6.3 VOF-RANS SIMULATIONS

In terms of using CFD for wave energy converters, VOF-RANS methods are popular because they include most physical effects important for WECs. Drag forces, added masses and radiation-diffraction interactions are all inherently included in the model approach. As it also supports overtopping and green-water effects, viscous contribution, and fully nonlinear or breaking waves it is a complete tool for evaluating floating WECs.

Non-linear response

The results of papers II, III and IV all show the same trend in nonlinear response amplitude dependence on the incoming wave height. The present contribution has served to further bring attention to this effect and its implications on WEC evaluation also in complete, realistic motion. The underlying reasons are generally attributed to the non-linear Froude-Krylov forces and the viscous drag damping [20]. But high-order contributions of other effects are also important. We argue that the best approach to gather full knowledge about the underlying causes for this effect is to use a hierarchical, numerical approach where a geometrically simple device is simulated using different numerical methods of varying complexity and completeness. An effort in this direction was presented by Eskilsson et al. in [53]. Detailed analysis of the local flow structure surrounding the device in resonating conditions should further be studied to understand the mechanisms of the damping.

An important step to clarify the steepness dependence of the response was recently taken by Rodriguez et al. In a pair of articles they presented experimental [135] and numerical [136] results showing strong high-order force components on a heaving box in two dimensions. They showed a detailed decomposition of the force contribution of diffraction and radiation in different orders of approximation. The loss of non-dimensional response amplitude for steeper waves was attributed to mainly viscous losses. We also stress the conclusion of Giorgi and Ringwood [69] who show that actively controlling the power take off serves to amplify the nonlinearities, and makes the use of high-fidelity models a neccessity for reliable results. Our modelling has served to show that nonlinear reduction of response amplitude is evident in both pitch and heave simultaneously for devices in small scale and in full scale. Previous simulations have been limited to heave only [1, 177].

Wave propagation using VOF

As noted by Chen et al. [30], wave propagation in CFD is not an easy task. However, the resolution required for a good wave resolution differs significantly between studies. Chen et al. showed very good results for wave propagation and recommended a resolution of at least 8 cells per wave height and 70 per wave length. The mesh sensitivity of Paper IV ranged from 22 – 36 cells per wave height and 113 – 227 cells per wave length, with mesh sizes in the range of 2 – 8 million cells. The mesh refinement study showed a 7 % difference in wave height and a 5 % difference in resulting response amplitude between the finest and the coarsest grid. Clearly, there are conflicting results regarding required resolution. The aspect ratio used in Paper IV was admittedly rather high, around 9 on average over the meshes used, and as noticed by Jacobsen et al. [85], this has a negative impact on the wave propagation performance. On the other hand, the free surface is in VOF simulations effectively a discontinuity in the volume fraction α, and is as such considered to be well resolved in finite volumes if it is contained within three cells [37]. Following the eight cell per wave height recommendation means that the width of the free surface is a minimum of 40 % of the wave height. It seems unlikely that a wave of that resolution will give well resolved loads on floating structures, nor accurately capture the kinematics of the wave.

The wave elevation can be measured in different ways. In the waves2Foam package [85], Jacobsen et al. implemented an integral approach, where the wave-height is constructed from the depth-integrated volume fraction. This is a robust measure of the mean disturbance of the free surface, but if not combined with visual inspection of the interface bad resolution of the air-water interface will not be detected. To explain with a crude but effective example: with this measure, a room full of ”fog” (50% water) and one half-full of water will give the same result for the position of the free surface. In the appended papers we have consistently used the iso-surface of a given volume fraction, typically $\alpha = 0.5$. An even more complete picture of the wave quality would be to present e.g. the 0.05, 0.5 and 0.95 percentile iso-lines to also show the bounds of the surface resolution.

A note on mesh motion

The refined region surrounding the free surface is essential to achieve a good VOF simulation. As shown in papers II and IV, a body region of refined meshes is also used. Combined motions of heave and pitch with a mesh deformation tied to the body puts high demands on the initial mesh so that regions of coarser mesh do not appear in the free surface approximation. Meshing a volume around the body with fine mesh quickly builds to the cell count, so this region is preferably minimised. This difficulty is not limited to the mesh deformation approach.

The passage of coarse cells through the water line is a challenge also for overset meshes, due to the fixed hierarchy between body meshes (the overset ones) and the background mesh [28]. Large amplitude mesh motion on a highly non-uniform background/outer mesh remains one of the main challenges for meshed methods in marine applications.

6.4 Coupled CFD-mooring analysis

The presence of the mooring system changes the hydrodynamic response of the structure significantly, especially in the surge direction. As the relative velocity between the fluid and the body changes, the governing Reynolds number and KC number are also affected. This complicates the analysis, but highlights the importance of including a model for realistic response to achieve a good estimation of the fluid loads on the hull.

Coupled mooring dynamics are now available in commercial fluid codes, and we expect many more CFD studies of moored WECs to emerge in the near future. Correct mooring response affects the stiffness of the device response, and using a high-fidelity model of the flow puts demands on every sub-system affecting the solution to be modelled with the same level of accuracy. This includes moorings and power take-off control.

The main simplification made in the coupled model is that the flow around the cable is not included in the mooring simulation. During the work of our first coupled study [124], using linear potential flow for the body motion, we found little difference in the results with and without wave motion acting on the mooring model. The effect of this on the simulation results is therefore judged to be small, and located in the region close to the surface. At greater depths, the wave velocities decrease and the assumption of still water becomes increasingly valid. The method of the coupling as such is however easily expanded to include a velocity sampling of the flow at the cable positions, to use as input to the Morison approximation of the forces.

6.5 The role of VOF-RANS in WEC design

The fatal drawback of VOF-RANS simulations is their computational cost. As an example, a full sea-state on a 14 million cell mesh of the Wave Dragon consumed 200 000 cpu hours [54]. This number should be seen as an indication only as it depends on many physical properties and numerical settings, of which the resolution of the wave region in the simulation is a contributing factor. An interesting route of development to bring down the computational effort of VOF-RANS models is using hybrid models, like suggested in [128]. Then only a small near-field flow, centered around the WEC is modeled using the full VOF-RANS approach, and high-order potential flow methods are used for the far-field wave propagation.

Under design conditions of extreme loading, such as at ultimate limit state (ULS) or accident limit state (ALS), the completeness of the VOF-RANS approach can provide crucial understanding of WEC response. However, the order of magnitude of the computational effort clearly states that these methods cannot be used for annual time-scale predictions of power production, nor are they at present to be considered for array modelling of more than a couple of devices.

A well known issue with experimental testing is the difference in the KC and Reynolds numbers of the model scale test and the full scale equivalent. This makes viscous forces more prominent in a small model than at larger scales. As wave-to-wire models use parametrised drag forces with calibrated coefficients, in consequence they will exaggerate the viscous damping in full scale, which makes numerical predictions of power production more uncertain. This is one of the key potential uses of CFD-based analysis for WEC application. There is no calibration of hydrodynamic coefficients involved in a validation using a VOF-RANS model. The exact accuracy of the model is a matter of discussion, but at its core VOF-RANS simulations are equally accurate (or erroneous) in full scale as in a model experiment. This opens up for the possibility to use VOF-RANS tools to ensure a better extrapolation of coefficients to full scale. In such a design loop, experiments would be made with the purpose of validating a VOF-RANS model of a device. Full-scale VOF-RANS simulations would then be used to establish regions of validity and suitable full-scale calibration of a wave-to-wire model. This design approach can thus generate both a better understanding of nonlinear effects in full scale, as well as increase the accuracy of power-prediction models of WECs.

7

Concluding remarks

Och lilla bäcken mot älven rinner
och älven rinner mot stora hav
Och aldrig någonsin mer man finner
vart lilla bäcken blev av
Allan Edvall

We have described the development of a numerical method for mooring cable dynamics, including $hp-$adaptive mesh refinement and snap load capturing capabilities. The mooring module, named Moody, was further coupled to a VOF-RANS solver in OpenFOAM [110] to simulate the motion of moored wave energy converters. The results from the coupled model showed how VOF-RANS simulations can be used to model realistic response of moored devices.

We showed that discontinuous Galerkin (DG) methods can be used to model mooring dynamics with high-order convergence for smooth solutions. Two DG formulations were presented, one using the local DG method (LDG) and one implementing the local Lax-Friedrich (LF) approximative Riemann solver with $hp-$adaptivity. Both formulations showed good comparison with experimental data, but adaptivity and shock-capturing schemes were more suitable to implement in the conservative formulation of the LF solver. The LF solver showed successful snap load capturing for both linear and nonlinear materials, as well as excellent agreement with experimental data. The problem of modelling ground interaction was highlighted, with emphasis on how the ground friction force dominates the damping of longitudinal tension waves. The cable formulation is at present without bending stiffness and without internal damping properties. The inclusion of these features are left as future work and are important for a more robust treatment of cable slack and of snap load propagation.

The snap load capturing capabilities of Moody constitute a first step towards being able to quantify the influence of snap loads on the integrity of marine cable structures. This includes both peak tension amplitude – affecting the maximum load – and how the tension shock propagates along the cable – having a direct impact on the fatigue damage estimation. The use of $hp-$adaptivity opens up the possibility to decrease extensive mesh convergence studies on the moorings and instead use a tolerance based simulation approach. Naturally, much more work on validation of the error indication and mesh adaptivity control is needed before this can be realised in practical engineering.

We also presented one of the first coupled mooring simulation using VOF-RANS simulations for wave energy applications. A coupling between OpenFOAM and the mooring dynamics software using the LDG method was established and validated. The response amplification of the WEC at resonance is sharply decreasing with an increasing wave steepness. Studies aiming to quantify the physical factors behind this effect are ongoing. We argue that VOF-RANS simulations with coupled moorings and power take off is a suitable approach to increase the quality of power prediction tools, especially in the transition from results on an experimental scale to its full scale equivalent. We conclude that predictions of the nonlinear response of WECs in the resonance region requires high-fidelity models of the WEC motion and the wave loads. Giorgi and Ringwood [69] arrive at the same conclusion from a control perspective, where using linear or weakly non-linear methods for body forces results in less beneficial control parameters and erroneous prediction of power production.

High-accuracy experimental test campaigns designed for CFD validation are still needed. We stress that these should involve realistic moorings and be at as large a scale as the experimental facility can manage. For the purpose of mooring validation, the scale of these experiments becomes very important. Small errors of measurement are amplified in the mooring signal at too small scales.

In conclusion, the models developed and tested in this thesis have not yet had impact on actual design of WECs. Nevertheless, the potential impact of coupled VOF-RANS methods for WEC design and a reliable tool for snap load prediction in mooring dynamics is large. Currently much effort is put towards bringing WEC concepts from prototype scale to full scale and array demonstration [150]. At the same time, it is evident from the literature and from the results presented in this thesis, that there is still much knowledge and understanding to be gained from careful monitoring and simulation of even a single, generic device. It is the stand-point of this thesis that the full range of computational methods for floating WECs should be used to evaluate a wide range of design parameters of a device, its mooring system, and its power take off, before going beyond laboratory scale. To use the numerical methods presented in this thesis can enable an efficient way to achieve the desirable development path of *performance before readiness* in the TRL-TPL matrix of [166]. The costs of field testing and prototype construction are very high, and the consequences of failure are devastating to both the development company and to the wave energy industry. It seems evident that the cost of using high-fidelity numerical tools in an early stage of development, to limit uncertainties and optimise the design, are dwarfed by the potential savings on all future offshore endeavours of the wave energy device.

REFERENCES

[1] E.B. Agamloh, A.K. Wallace, and A. von Jouanne. Application of fluid-structure interaction of an ocean wave energy extraction device. *Renewable Energy*, 33(4):748–757, 2008.

[2] International Energy Agency. Key world energy statistics. Technical report, IEA, 2016. Available www.iea.org.

[3] International Renewable Energy Agency. Wave energy technology brief. Technical report, IRENA, 2014. Available www.irena.org.

[4] S. Aliabadi, J. Abedi, and B. Zellars. Parallel finite element simulation of mooring forces on floating objects. *Numer. Meth. Fluids*, 41:809–822, 2003. DOI:10.1002/fld.459.

[5] M. Alves and A. Sarmento. Non-linear and viscous analysis of the diffraction flow in OWC wave power plants. In *Proc. 16th International Offshore and Polar Engineering Conference*, San Francisco, USA, 2006.

[6] M. Anbarsooz, M. Passandideh-Fard, and M. Moghiman. Numerical simulation of a submerged cylindrical wave energy converter. *Renewable Energy*, 64:132–143, 2014.

[7] ANSYS Inc. *AQWA Theory Manual 15.0*, 2013.

[8] D. N. Arnold. An interior penalty finite element method with discontinuous elements. *SIAM J. Numer. Anal.*, 19:724–760, 1982.

[9] D. N. Arnold, F. Brezzi, B. Cockburn, and L.D. Marini. Unified analysis of discontinuous Galerkin methods for elliptic problems. *SIAM J. Numer. Anal.*, 39:1749–1779, 2002.

[10] A. Babarit and G. Delhommeau. Theoretical and numerical aspects of the open source BEM solver NEMOH. In *Proc. 11th European Wave and Tidal Energy Conference*, Nantes, France, 2015.

[11] A. Babarit, J. Hals, M.J. Muliawan, A. Kurniawan, T. Moan, and J. Krokstad. Numerical benchmarking study of a selection of wave energy converters. *Renewable Energy*, 41:44–63, 2012.

[12] F. Bassi and F. Rabay. A high-order accurate finite element method for the numerical solution of the compressible Navier-Stokes equations. *J. Comp. Phys.*, 131:267–279, 1997.

[13] K.J. Bathe and E.L. Wilson. *Num. Meth. in Finite Element Analysis*. Prentice Hall, Inc., Englewood Cliffs, New Jersey, 1976.

[14] BBC. Available http://www.bbc.com/news/uk-scotland-scotland-business-34901133.

[15] N. Bengtsson and V. Ekström. *Seaflex. The buoy mooring system. Increase Life Cycle and Decrease Cost for Navigation Buoys-Extension of Life by Reduction of Maintenance for Mooring Products*. Seaflex Energy Systems AB.

[16] L. Bergdahl. Review of research in Sweden. In *Wave energy R&D workshop: Commission of the European Communities.*, Cork, Ireland, 1992.

[17] L. Bergdahl, J. Palm, C. Eskilsson, and J. Lindahl. Dynamically scaled model experiment of a mooring cable. *J. Marine Science and Technology*, 4(5), 2016.

[18] M. Berger, M.J. Aftosmis, and S.M. Murman. Analysis of slope limiters on irregular grids. Technical report, American Institute of Aeronautics and Astronautics, 2005.

[19] P. Bernard. *Discontinuous Galerkin methods for Geophysical Flow Modeling*. PhD thesis, Ecole polytechnique de Louvain, 2008.

[20] M.A. Bhinder, A. Babarit, L. Gentaz, and P. Ferrant. Assessment of viscous damping via 3D-CFD modelling of a floating wave energy device. In *Proc. 9th European Wave and Tidal Energy Conference*, Southampton, United Kingdom, 2011.

[21] M.A. Bhinder, A. Babarit, L. Gentaz, and P. Ferrant. Potential time domain model with viscous correction and CFD analysis of a generic surging floating wave energy converter. *International Journal of Marine Energy*, 10:70–96, 2015.

[22] Bloomberg. Available https://www.bloomberg.com/news/articles/2013-04-03/wavebob-shuts-down-after-failing-to-raise-funds-find-partner.

[23] J. Brooke. *Wave Energy Conversion*. Elsevier, 2003.

[24] D.T. Brown and S. Mavrakos. Comparative study on mooring line dynamic loading. *Marine Structures*, 12:131–151, 1999.

[25] B. Buckham, F. Driscoll, and M. Nahon. Development of a finite element cable model for use in low-tension dynamics simulations. *Journal of Applied Mechanics*, 71:476–485, 2004.

[26] F. Budal and J. Falnes. A resonant point-absorber of ocean wave power. *Nature*, 256:478–479, 1975.

[27] K. Budal and J. Falnes. *Interacting Point Absorbers with Controlled Motion, Power from Sea Waves*. Academic Press, 1980.

[28] CD-Adapco (Siemens). *Star-ccm+, User Guide*, 2016.

[29] S.K. Chakrabarti. *Hydrodynamics of Offshore Structures*. Computational Mechanics Publications. Springer-Verlag, 1987.

[30] L.F. Chen, J. Zang, A.J. Hillis, G.C.J. Morgan, and A.R. Plummer. Numerical investigation of wave-structure interaction using openfoam. *Ocean Engineering*, 88:91–109, 2014.

[31] B. Cockburn and C.W. Shu. TVB Runge-Kutta local projection discontinuous Galerkin finite element method for conservation laws iii: One dimensional systems. *J. Comp. Phys.*, 84:90–113, 1989.

[32] B. Cockburn and C.W. Shu. TVB Runge-Kutta local projection discontinuous Galerkin finite element method for scalar conservation laws ii: General framework. *Math. Comp.*, 52:411–435, 1989.

[33] B. Cockburn and C.W. Shu. TVB Runge-Kutta local projection discontinuous Galerkin finite element method for conservation laws iv: The multidimensional case. *Math. Comp.*, 54:545–581, 1990.

[34] B. Cockburn and C.W. Shu. The Runge-Kutta local projection p^1-discontinuous Galerkin method for scalar conservation laws. *Mathematical Modelling and Numerical Analysis*, 25(3):337–361, 1991.

[35] B. Cockburn and C.W. Shu. The local discontinuous Galerkin method for time-dependent convection-dominated systems. *SIAM J. Numer. Anal.*, 35(6):2440–2463, 1998.

[36] B. Cockburn and C.W. Shu. The Runge-Kutta discontinuous Galerkin finite element method for conservation laws v: Multidimensional systems. *J. Comp. Phys.*, 141:199–224, 1998.

[37] B. Cockburn and C.W. Shu. Runge-Kutta discontinuous Galerkin methods for convection-dominated problems. *J. Sci. Comp.*, 16:173–261, 2001.

[38] R.G. Coe and V.S. Neary. Review of methods for modeling wave energy converter survival in extreme sea states. In *Proc. 2nd Marine Energy Technology Symposium*, Seattle, USA, 2014.

[39] A. Copping, N. Sather, L. Hanna, J. Whiting, G. Zydlewski, G. Staines, A. Gill, I. Hutchison, A. OHagan, T. Simas, J. Bald, Sparling C., J. Wood, and E. Masden. Annex IV 2016 State of the Science Report: Environmental Effects of Marine Renewable Energy Development Around the World., 2016.

[40] J. Cruz. *Ocean Wave Energy, Current Status and Future Perspectives*. Springer verlag, 2008.

[41] W.E. Cummins. The impulse response function and ship motions. *Schiffstechnik*, 9:101–109, 1962.

[42] J. Davidson, M. Cathelain, L. Guillemet, T. Le Huec, and J. Ringwood. Implementation of an OpenFOAM numerical wave tank for wave energy experiments. In *Proc. 11th European Wave and Tidal Energy Conference*, Nantes, France, 2015.

[43] J. Davidson, S. Giorgi, and J.V. Ringwood. Linear parametric models for ocean wave energy converters identified from numerical wave tank experiments. *Ocean Engineering*, 103:31–39, 2015.

[44] A.H. Day, A. Babarit, A. Fontaine, Y.-P. He, M. Kraskowski, M. Murai, I. Penesis, F. Salvatore, and H.-K. Shin. Hydrodynamic modelling of marine renewable energy devices: A state of the art review. *Ocean Engineering*, 108:46–69, 2015.

[45] R.G. Dean and R.A. Dalrymple. *Water Wave Mechanics for Engineers and Scientists*. World Scientific, 1991.

[46] Det Norske Veritas. *Position Mooring*, 2010. Offshore standard DNV-OS-301.

[47] M. Dhanak and X. Nikolaos. *Handbook on Ocean Engineering*. Springer verlag, 2016.

[48] DNV GL. *SESAM Theory Manual for DeepC 3.0*, 2014.

[49] EMEC. *Eurpoean Marine Energy Centre Homepage*, 2017. Available http://www.emec.org.uk/marine-energy/wave-developers/.

[50] A.P. Engsig-Karup, H.B. Bingham, and O. Lindberg. An efficient flexible-order model for 3D nonlinear water waves. *J. Comp. Phys.*, 228:2100–2118, 2009.

[51] A. Ensig-Karup. *Unstructured Nodal DG-FEM Solution of High-order Boussinesq-type Equations*. PhD thesis, Technical University of Denmark, 2006.

[52] C. Eskilsson. An hp-adaptive discontinuous Galerkin method for shallow water flows. *International Journal of Numerical Methods in Fluids*, 67:1605–1623, 2011.

[53] C. Eskilsson, J. Palm, A.P. Ensig-Karup, U. Bosi, and M. Ricchiuto. Wave induced motions of point-absorbers: an hierarchical investigation of hydrodynamic models. In *Proc. 11th European Wave and Tidal Energy Conference*, Nantes, France, 2015.

[54] C. Eskilsson, J. Palm, J.P Kofoed, and E. Friis-Madsen. CFD study of the overtopping discharge rate of the Wave Dragon wave energy converter. In C. Guedes Soares, editor, *Renewable Energies Offshore*, pages 287–294. Taylor & Francis Group, November 2014.

[55] D. V. Evans. A theory for wave-power absorption by oscillating bodies. *J. Fluid Mech.*, 77:1–25, 1976.

[56] A. Falcao. Wave energy utilization: A review of the technologies. *Renewable and Sustainable Energy Reviews*, 14:899–918, 2010.

[57] J. Falnes. A review of wave-energy extraction. *Marine Structures*, 20:185–201, 2007.

[58] O.M. Faltinsen. *Sealoads on Ships and Offshore Structures*. Cambridge University Press, 1990.

[59] F. Ferri and J. Palm. Implementation of a dynamic mooring solver (MOODY) into a wave to wire model of a simple WEC. Technical report, Department of Civil Engineering, Aalborg University, 2015.

[60] J. Fitzgerald. *Position Mooring of Wave Energy Converters*. PhD thesis, Chalmers University of Technology, 2009.

[61] J. Fitzgerald and L. Bergdahl. Considering mooring cables for offshore wave energy converters. In *Proc. 7th European Wave and Tidal Energy Conference*, Oporto, Portugal, 2007.

[62] J. Fitzgerald and L. Bergdahl. Including moorings in the assessment of a generic offshore wave energy converter: a frequency domain approach. *Marine Structures*, 21:23–46, 2008.

[63] J. Fitzgerald and B Bolund. Technology readiness for wave energy projects; ESB and Vattenfall classification system. In *Proc. 4th International Conference on Ocean Energy*, Dublin, Ireland, 2012.

[64] Flow3D. *Flow3D Homepage*. Available http://www.flow3d.com.

[65] M. Folley. *Numerical Modelling of Wave Energy Converters, State-Of-The-Art Techniques for Single Devices and Arrays*. Elsevier Inc., 2016.

[66] Ocean Energy Forum. Ocean Energy Strategic Roadmap 2016, building ocean energy for Europe, 2016.

[67] P. Frigaard and M. Christensen. An absorbing wave-maker based on digital filters. In *Proc. 24th International Conference on Coastal Engineering*, Kobe, Japan, 1994.

[68] I.J. Fylling and T.P. Wold. Cable dynamics - comparison of experimental and analytical results. The Ship Research Institute of Norway, 1979.

[69] S. Giorgi and J. Ringwood. Implementation of latching control in a numerical wave tank with regular waves. *J. Ocean Eng. Mar. Energy*, 2:211–226, 2016.

[70] DNV GL. *WAVEDYN. Wave energy converter modelling tool*. DNV GL, 2016.

[71] J. Gobat. *The Dynamics of Geometrically Compliant Mooring Systems*. PhD thesis, Massachusets Institute of Technology and Woods Hole Oceanographic Institution, 2000.

[72] J.I. Gobat and M.A. Grosenbaugh. Dynamics in the trouchdown region of catenary moorings. In *Proc.11th International Offshore and Polar Engineering Conference*, Stavanger, Norway, 2001.

[73] S.K. Godunov. Finite difference methods for the computation of discontinuous solutions of the equations of fluid dynamics. *Mat. Sb.*, 47:271–306, 1959.

[74] J.E. Goeller and P.A. Laura. Analytical and experimental study of the dynamic response of segmented cable systems. *Journal of Sound and Vibration*, 18:311–324, 1971.

[75] G. Hagerman. *Wave Power*. John Wiley and sons Inc., 1995.

[76] J. Hals, G.S. Asgeirsson, E. Hjalmarsson, J. Maillet, P. Moller, P. Pires, M. Guerinel, and M. Lopes. Tank testing of an inherently phase-controlled wave energy converter. *Int. J. of Marine Energy*, 15:68–84, 2016.

[77] P. Hansbo and M. G. Larson. Discontinuous Galerkin methods for incompressible and nearly incompressible elasticity by Nitsches method. *Comput. Methods Appl. Mech. Engrg.*, 191:1895–1908, 2002.

[78] V. Harnois. *Analysis of Highly Dynamic Mooring Systems: Peak Mooring Loads in Realistic Sea Conditions*. PhD thesis, University of Exeter, 2014.

[79] R. E. Harris, L. Johanning, and J. Wolfram. Mooring systems for wave energy converters: A review of design issues and choices. In *Proc. 3rd International Conference on Marine Renewable Energy*, Blyth, UK, 2004.

[80] C.M. Hennessey, N.J. Pearson, and R.H. Plaut. Experimental snap loading of synthetic ropes. *Shock and Vibration*, 12:163–175, 2005.

[81] P. Higuera, J.L. Lara, and I.J. Losada. Realistic wave generation and active wave absorption for Navier-Stokes models application to OpenFOAM. *Coastal Engineering*, 71:102–118, 2013.

[82] T. Hou and P.G. Le Floch. Why nonconservative schemes converge to wrong solutions: Error analysis. *Mathematics of Computation*, 1994.

[83] P. Houson, D. Schtzau, and T. P. Wihler. An hp-adaptive mixed discontinuous Galerkin FEM for nearly incompressible linear elasticity. *Comp. Meth. Appl. Mech. Engineering*, 2006.

[84] A. Iturrioz, R. Guanche, J.K. Lara, C. Vidal, and I.J. Losada. Validation of OpenFOAM for oscillating water column three-dimensional modeling. *Ocean Engineering*, 107:222–236, 2015.

[85] N.G. Jacobsen, D.R. Fuhrman, and J. Fredsøe. A wave generation toolbox for the open-source CFD library: OpenFOAM®. *Int. J. for Numerical Methods in Fluids*, 70:1073–1088, 2012.

[86] L. Johanning, G. Smith, and J. Wolfram. Measurements of static and dynamic mooring line damping and their importance for floating WEC devices. *Ocean Engineering*, 34:1918–1934, 2007.

[87] G. E. Karniadakis and S. Sherwin. *Spectral/hp Element Methods for CFD*. Oxford University Press, New York, Oxford, 2nd edition edition, 2003.

[88] M. Käser and M. Dumbser. An arbitrary high-order discontinuous Galerkin method for elastic waves on unstructured meshes i. The two-dimensional isotropic case with external source terms. *Geophys. J. Int.*, 166:855–877, 2006.

[89] J.W. Kim, R. Izarra, H. Jang, J. Kyong, and J. O'Sullivan. An application of the eom-based numerical basin to dry-tree semisubmersible design. In *Proc. 19th Offshore Symposium*, Houston, USA, 2014.

[90] A. Klöckner, T. Warburton, and J. S. Hesthaven. Viscous shock capturing in a time-explicit discontinuous Galerkin method. *Math. Model. Nat. Phenom.*, X:1–27, 2011.

[91] L. Krivodonova, J. Xin, J.-F. Remacle, N. Chevaugeon, and J. Flaherty. Shock detection and limiting with discontinuous Galerkin methods for hyperbolic conservation laws. *J. Appl. Num. Math.*, 48:323–338, 2004.

[92] V. Krivtsov, B. Linfoot, and R.E. Harris. Effects of the shape and size of a mooring line surface buoy on the mooring load of wave energy converters. *J. of Chongqing Univ.*, 11:1–4, 2012.

[93] L. Larsson, F. Stern, and M. Visonneau. *Numerical Ship Hydrodynamics*. Springer, New York, 2010.

[94] M. Lawson, Y-H. Yu, A. Neleesen, K. Ruehl, and C. Michelen. Implementing nonlinear buoyancy and excitation forces in the wec-sim wave energy converter modeling tool. In *Proc. 33rd International Conference on Ocean, Offshore and Arctic Engineering*, 2014.

[95] P. D. Lax and B. Wendroff. Systems of conservation laws. *Comm. Pure Appl. Math.*, 13:217–237, 1960.

[96] Y. Li and M. Lin. Regular and irregular wave impacts on floating body. *Ocean Engineering*, 42:93–101, 2012.

[97] Y. Li and Y.H. Yu. A synthesis of numerical methods for modeling wave energy converter-point absorbers. *Renewable and Sustainable Energy Reviews*, 16:4352–4364, 2012.

[98] P. Lin and P. Liu. A numerical study of breaking waves in the surf zone. *J. Fluid Mech.*, 359:239–264, 1998.

[99] J. Lindahl. Modellförsök med en förankringskabel. Technical Report Report Series A:12, Chalmers University of Technology, 1985.

[100] Y. Liu. Dynamics and extreme value problems for moored floating platforms. Technical Report Report Series A:29, Chalmers University of Technology, 1998.

[101] K. Ma, A. Duggal, P. Smedley, D. L'Hostis, and H. Shu. A historical review on integrity issues of permanent mooring systems. In *Proc. Offshore Technology Conference*, Houston, Texas, USA, 2013.

[102] S. Mahji and R. D'Souza. Application of lessons learned from field experience to design, installation and maintenance of FPS moorings. In *Proc. Offshore Technology Conference*, Houston, Texas, USA, 2013.

[103] S.A. Mavrakos, V.J. Papazoglou, M.S. Triantafyllou, and J. Hatjigeorgiou. Deep water mooring dynamics. *Marine Structures*, 9:181–209, 1996.

[104] C. C. Mei. Power extraction from water waves. *J. Ship Res.*, 20:63–66, 1976.

[105] A. Montano, M. Reselli, and R. Sacco. Numerical simulation of tethered buoy dynamics using mixed finite elements. *Comp. Meth. Appl. Mech. Eng.*, 196:4117–4129, 2007.

[106] J.R. Morison, M.P. O'Brien, J.W. Johnson, and S.A. Schaaf. The force exerted by surface waves on piles. *Petroleum Transactions, Amer. Inst. Mining Engineers*, 186:149–154, 1950.

[107] J. N. Newman. The interaction of stationary vessels with regular waves. In *Proc. 11th Sym. Naval Hydrodynam.*, London, UK, 1976.

[108] R. Nicholls-Lee, A. Walker, S. Hindley, and R. Argall. Coupled multi-phase CFD and transient mooring analysis of the floating wave energy converter OWEL. In *Proc. 32nd International Conference on Ocean, Offshore and Arctic Engineering*, Nantes, France, 2013.

[109] A.M. via Ocean Energy Systems O'Hagen. Consenting processes for ocean energy, update on barriers and recommendations, 2016.

[110] OpenCFD Ltd. *OpenFOAM Homepage*, 2014. Available http://www.openfoam.org.

[111] Orcina Inc. *OrcaFlex manual – version 9.5a*, 2012.

[112] J.P. Ortiz, H. Bailey, B. Buckham, and C. Crawford. Surrogate based design of a mooring system for a self-reacting point absorber. In *Proc. 25th International Offshore and Polar Engineering Conference*, Kona,Hawaii, 2015.

[113] J. Palm. *Connecting OpenFOAM with MATLAB*, 2012. Available http://www.tfd.chalmers.se/~hani/kurser/OS_CFD_2012/.

[114] J. Palm. Developing Computational Methods for Moored Floating Wave Energy Devices. Technical report, Department of Shipping and Marine Technology, Chalmers University of Technology, 2014. Lic.Eng. Thesis. Report No. 14:151.

[115] J. Palm and C. Eskilsson. *MOODY, User's manual version m-1.0*, 2014. Avaliable www.sdwed.civil.aau.dk.

[116] J. Palm, C. Eskilsson, and L. Bergdahl. Mooring cable simulations with snap load capturing for wave energy applications. In C. Guedes Soares, editor, *Progress in Renewable Energies Offshore*, pages 695–701. Taylor & Francis Group, October 2016.

[117] J. Palm, C. Eskilsson, and L. Bergdahl. An hp-adaptive discontinuous Galerkin method for modelling snap loads in mooring cables. *Submitted*, pages 1–32, 2017.

[118] J. Palm, C. Eskilsson, G. Paredes, and L. Bergdahl. CFD simulations of a moored floating wave energy converter. In *Proc. 10th European Wave and Tidal Energy Conference*, Aalborg, Denmark, 2013.

[119] J. Palm, C. Eskilsson, G. Paredes, and L. Bergdahl. CFD study of a moored floating cylinder: Comparison with experimental data. In C. Guedes Soares, editor, *Renewable Energies Offshore*, pages 913–920. Taylor & Francis Group, November 2014.

[120] J. Palm, C. Eskilsson, G. Paredes, and L. Bergdahl. Coupled mooring analysis for floating wave energy converters using CFD: Formulation and validation. *Int. J. of Marine Energy*, 16:83–99, 2016.

[121] J. Palm, G. Paredes, C. Eskilsson, F. Taveira-Pinto, and L. Bergdahl. Simulation of mooring cable dynamics using a discontinuous Galerkin method. In *Proc. 5th International Conference on Computational Methods in Marine Engineering*, Hamburg, Germany, 2013.

[122] G. Paredes. *Study of Mooring Systems for Offshore Wave Energy Converters*. PhD thesis, University of Porto, 2016.

[123] G. Paredes, L. Bergdahl, J. Palm, C. Eskilsson, and F. Pinto. Station keeping design for floating wave energy devices compared to floating offshore oil and gas platforms. In *Proc. 10th European Wave and Tidal Energy Conference*, Aalborg, Denmark, 2013.

[124] G. Paredes, C. Eskilsson, J. Palm, L. Bergdahl, L. Leite, and F. Pinto. Experimental and numerical modeling of a moored, generic wave energy converter. In *Proc. 10th European Wave and Tidal Energy Conference*, Aalborg, Denmark, 2013.

[125] G. Paredes, J. Palm, C. Eskilsson, L. Bergdahl, and F. Taveira-Pinto. Numerical modelling of mooring systems for floating wave energy converters. In *8as Jornadas de Hidráulica, Recursos Hídricos e Ambiente*, Porto, 2014. Faculdade de Engenharia da Universidade do Porto.

[126] G. Paredes, J. Palm, C. Eskilsson, L. Bergdahl, and F. Taveira-Pinto. Experimental investigation of mooring configurations for wave energy converters. In *Proc. 11th European Wave and Tidal Energy Conference*, Nantes, France, 2015.

[127] G. Paredes, J. Palm, C. Eskilsson, L. Bergdahl, and F. Taveira-Pinto. Experimental investigation of mooring configurations for wave energy converters. *Int. J. of Marine Energy*, 15:56–67, 2016.

[128] B.T. Paulsen, H. Bredmose, and H.B. Bingham. An efficient domain decomposition strategy for wave loads on surface piercing circular cylinders. *Coastal Engineering*, 86:57–76, 2014.

[129] A. Pecher and J. P. Kofoed. *Handbook of Ocean Wave Energy*. Springer verlag., 2017.

[130] M. Penalba and J. Ringwood. A review of wave-to-wire models for wave energy converters. *MDPI, Energies*, 9:1–45, 2016.

[131] P. Persson and J. Peraire. Sub-cell shock capturing for discontinuous Galerkin methods. In *Proc. 44th AIAA Aerospace Sciences Meeting and Exhibit*, 2006.

[132] S.B. Raknes, Deng X., Y. Bazilevs Y., D.J. Benson, Mathisen K.M., and T. Kvamsdal. Isogeometric rotation-free bending-stabilized cables: Statics, dynamics, bending strips and coupling with shells. *Comp. Meth. Appl. Mech. Eng.*, 263:127–143, 2013.

[133] W. H. Reed and T. R. Hill. Triangular mesh methods for the neutron transport equation. Technical Report LA-UR-73.739, Los Alamos Scientific Laboratory, 1973.

[134] M.P. Retes, A. Merigaud, J.P. Gilloteaux, and J. Ringwood. Nonlinear froude-krylov force modelling for two heaving wave energy point absorbers. In *Proc. 11th European Wave and Tidal Energy Conference*, Nantes, France, 2015.

[135] M. Rodrigues and J. Spinneken. A laboratory study on the loading and motion of a heaving box. *J. of Fluids and Structures*, 64:107–126, 2016.

[136] M. Rodrigues, J. Spinneken, and C. Swan. Nonlinear loading of a two-dimensional heaving box. *J. of Fluids and Structures*, 60:80–96, 2016.

[137] D. Ross. *Power from the Waves*. Oxford university press, 1995.

[138] E.J. Routh. *An elementary treatise on the dynamics of a system of rigid bodies*. Cambridge: Macmillan and Co., 1860.

[139] H. Rusche. *Computational Fluid Dynamics of Dispersed Two-Phase Flow at High Phase Fractions.* PhD thesis, Imperial College London, 2003.

[140] Safetec. Causal relationships and measures associated with structural and maritime incidents on the norwegian continental shelf. Technical report, Petroleum Safety Authority Norway, 1973.

[141] S. H. Salter. Wave power. *Nature*, 249, 1974.

[142] S. H. Salter, J. R. M. Taylor, and N.J. Caldwell. Power conversion mechanisms for wave energy. *Proc. Instn Mech Engrs Part M*, 216, 2002.

[143] A. Savin, O. Svensson, and M. Leijon. Azimuth-inclination angles and snatch load on a tight mooring system. *Ocean Engineering*, 40:40–49, 2012.

[144] P. Schmitt and B. Elsaesser. On the use of OpenFOAM to model oscillating wave surge converters. *Ocean Engineering*, 108, 2015.

[145] Seabased AB. *Seabased Homepage*, 2017.

[146] K. Spak, G. Agnes, and D. Inman. Cable modeling and internal damping developments. *Applied Mechanics Reviews, ASME*, 65(1), 2013.

[147] T. Suhara, W. Koteryama, F. Tasai, and Hiyama. Dynamic behavior and tension of oscillating mooring chain. In *Proceedings of the 13th Offshore technology conference (OTC)*, 1981.

[148] P.T. Sweby. High resolution schemes using flux limiters for hyperbolic conservation laws. *SIAM Journal on Numerical Analysis*, 21(5):995–1011, 1984.

[149] Ocean Energy Systems. Annual report. Implementing agreement on Ocean Energy Systems, 2015.

[150] European Technology and Innovation Platform for Ocean Energy. Strategic research agenda for ocean energy. Brussels, Belgium, 2016.

[151] the Scotsman. Available http://www.scotsman.com/news/pelamis-had-debts-of-15m-following-collapse-1-3690586.

[152] A. Tjavaras. *The Dynamics of Highly Extensible Cables*. PhD thesis, Massachusetts Institute of Technology, 1996.

[153] E.F. Toro. *Shock-Capturing Methods for Free-Surface Shallow Flows*. Wiley and Sons, Ltd, 2001.

[154] M.S. Triantafyllou, A. Bliek, and H. Shin. Dynamic analysis as a tool for open-sea mooring system design. *SNAME Transactions*, 93:302–324, 1985.

[155] M.S. Triantafyllou and C.T. Howell. Nonlinear impulsive motion of low-tension cables. *J. Eng. Mech.*, 118(4):807–830, 1992.

[156] M.S. Triantafyllou and C.T. Howell. Dynamic response of cables under negative tension: An ill-posed problem. *J. Sound and Vibration*, 173(4):433–447, 1994.

[157] P. Troch and J. De Rouck. An active wave generatingabsorbing boundary condition for VOF type numerical model. *Coastal Engineering*, 38:223–247, 1999.

[158] I. Tsukrov, O. Eroshkin, W. Paul, and Celikkol B. Numerical modeling of nonlinear elastic components of mooring systems. *Int. J. Oceanic Engineering*, 30(1):37–46, 2005.

[159] A. Uihlein and D. Magagna. Wave and tidal current energy a review of the current state of research beyond technology. *Renewable and Sustainable Energy Reviews*, 58:1070–1081, 2016.

[160] B. van Leer. Towards the ultimate conservative difference scheme. v. a second-order sequel to godunovs method. *J. Comp. Phys.*, 32:101–136, 1979.

[161] P. Vicente. *Moorings of Floating Point Absorber Wave Energy Converters in Arrays*. PhD thesis, INSTITUTO SUPERIOR TECNICO, 2016.

[162] P. Vicente, A. Falcao, L. Gato, and P. Justino. Dynamics of arrays of floating point-absorber wave energy converters with inter-body and bottom slack-mooring connections. *Ocean Engineering*, 31:267–281, 2009.

[163] T.S. Walton and H. Polachek. Calculation of transient motion of submerged cables. *Math. Comp.*, 14:27–46, 1959.

[164] WAMIT Inc. *WAMIT User Manual (version6.4)*.

[165] Waves 4 Power AB. *Waves 4 Power Homepage*, 2017.

[166] J. Weber, R. Costello, and J. Ringwood. Wec technology readiness and performance matrix - finding the best research technology development trajectory. In *Proc. ICOE 2012*, Dublin, Ireland, 2012.

[167] H.G. Weller, G. Tabor, H. Jasak, and C. Fureby. A tensorial approach to CFD using object oriented techniques. *Comp. in Physics*, 12:620–631, 1998.

[168] S. Weller, P. Davies, A.W. Vickers, and L. Johanning. Synthetic rope responses in the context of load history: Operational performance. *Ocean Engineering*, 83:111–124, 2014.

[169] S. Weller, P. Davies, A.W. Vickers, and L. Johanning. Synthetic rope responses in the context of load history: The influence of aging. *Ocean Engineering*, 96:192–204, 2015.

[170] S. Weller, L. Johanning, and P. Davies. Best practice report - mooring of floating marine renewable energy devices: Deliverable 3.5.3 from the MERiFIC project, 2013.

[171] L. C. Wilcox, G. Stadler, C. Burstedde, and O. Ghattas. A high-order discontinuous Galerkin method for wave propagation through coupled elasticacoustic media. *J. Comp. Phys.*, 229:9373–9396, 2010.

[172] H.A. Wolgamot and C.J. Fitzgerald. Nonlinear hydrodynamic and real fluid effects on wave energy converters. In *Proc. IMechE Part A: J Power and Energy*, 2015.

[173] V. Yakhot, S.A. Orszag, S. Thangam, T.B. Gatski, and C.G. Speziale. Development of turbulence models for shear flows by a double expansion technique. *Physics of Fluids A*, 4(7):1510–1520, 1992.

[174] S. Yang, J. Ringsberg, E. Johnson, Z. Hu, and J. Palm. A comparison of coupled and de-coupled simulation procedures for the fatigue analysis of wave energy converter mooring lines. *Ocean Engineering*, 117:332–345, 2016.

[175] S.H. Yang. *Analysis of Fatigue Characteristics in Mooring Lines and Low Voltage Cables for Wave Energy Converters*, 2016. Lic.Eng. Thesis. Report No. 16:163.

[176] Y. Yu and Y. Li. Preliminary results of a RANS simulation for a floating point absorber wave energy system. In *Proc. 30th Interational Conference on Ocean, Offshore and Arctic Engineering*, Rotterdam, The Netherlands, June 2011.

[177] Y.H. Yu and Y. Li. Reynolds-averaged Navier-Stokes simulation of the heave performance of a two-body floating-point absorber wave energy system. *Computers and Fluids*, 73:104–114, 2013.

[178] Y.H. Yu, J. Van Rij, and M. Lawson. Preliminary wave energy converters extreme load analysis. In *Proc. 34th Interational Conference on Ocean, Offshore and Arctic Engineering*, St John's, Canada, June 2015.